Sea Level Rise Around the Dutch Coast: Past Changes and Future Scenarios (V2.0)

March 24, 2008

Prepared for:
Pier Vellinga
Wageningen University and Research Centre
The Netherlands
As Input to the Assessment for the Delta Committee

Prepared by:
Hans-Peter Plag,
8720 Rainbow Trout Ct.
Reno, NV 89557
USA

REVISION HISTORY		
Rev.	**Description**	**Date**
1	Version 1.0, incomplete draft	January 23, 2008
2	Version 1.1, complete draft	January 28, 2008
3	Version 2.0	March 25, 2008

About this document

This document is a contribution to the assessment of future sea level rise currently underway for the Delta Committee of the Dutch Parliament. This committee is charged with the drawing up of scenarios for spatial planning and infrastructure and is asked by the Dutch Government to present the full range of plausible sea level change scenarios (inclusive worse case scenarios). It is explicitly interested in the most likely scenarios, as well as the upper bound of the scenarios, that is the highest 5 to 10 % low probability/high impact sea level rise and storm surge scenarios.

A starting point for the work are the global sea level rise scenarios of the IPCC AR4 report. However, there is considerable scientific debate about the present and future rate of melting of ice sheets, and this needs to be addressed carefully. Therefore, the contributors to the assessment were asked to consider the following questions (text slightly modified by the author):

1. Can the probability density functions (PDFs) of global temperature as presented in IPCC Group I report (page 808, Fig 10.28) be translated into PDFs of the global sea level rise for the year 2050, 2100, 2200?
2. If it is too difficult to construct the above mentioned PDFs, could the author give a best personal scientific judgement about the mean $\mu = X_2$ and the means of the extreme values X_1, and X_3, the lower and upper bound respectively (see the Figure below) for the year 2050, 2100, 2200? (still referring to global sea level rise). If preferred, band of values can be used instead of single value, especially for the extreme bounds.
3. Can the full range of possible futures regarding the effect of melting of the Greenland and Antarctic ice sheets on the global sea level be explictly be stated? Can this be expressed in terms of mean value and extremes as in the previous question?
4. At regional level, how will climate change and sea level rise affect the mean sea levels in the North Sea in the year 2050, 2100, 2200?
5. What are the author's argued views about the effect of global warming on the maximum wind velocity, storm surge levels and wave heights and what about the possible changes in the (the for set up along the Netherlands shores) most relevant wind directions during extreme storms in the North sea area.

The present document focuses mainly on question 4 (Q4). However, based on an analysis of the factors contributing to global and regional/local sea level, answers concerning Q1, Q2 and Q3 are also addressed.

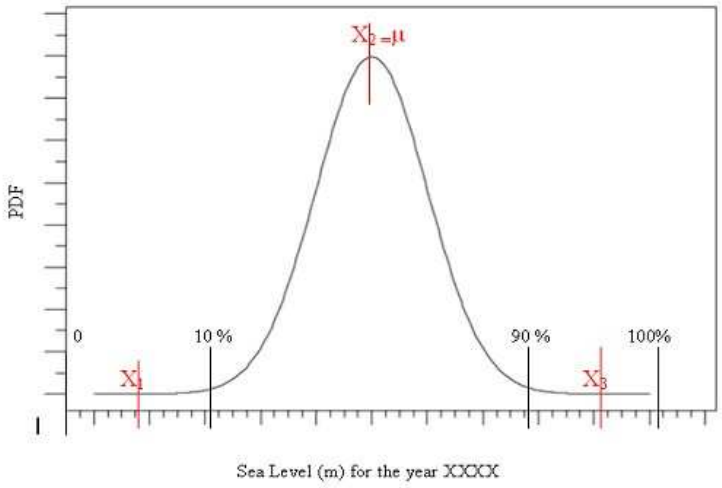

Contents

1 Introduction

The variable relevant for the impact of sea level rise on The Netherlands is relative sea level or, as is preferred here, *Local Sea Level* (LSL). At any coastal location, LSL is influenced by a number of processes with spatial scales from local to global. Each of these processes has its own characteristic spatial and temporal scales. With respect to future changes, each process is associated with its own *Probability Density Function* (PDF) distribution, which in most cases is geographically and temporally variable. Establishing a combined PDF for LSL at a given location will therefore be extremely difficult if not impossible. What can be done is to consider projection of plausible trajectories of future sea level for a wide range of forcing scenarios, similar to the approach taken for the assessment of future climate change (see, e.g., Meehl et al., 2007). However, this approach requires detailed knowledge of the relation between forcing on a wide range of spatial and temporal scales and LSL at a specific location. Consequently, in order to provide projections of future LSL, it is necessary to understand the forcing mechanisms of LSL variations and secular change.

In the following, we will first introduce LSL as the relevant impact parameter in the context of the anticipated climate change. We will then establish an equation linking LSL to the various forcing processes and emphasize the complex nature of this variable. We will split up this equation into a high-frequency and a low-frequency part and mainly focus on the low-frequency part. Based on an empirical approximation, we will test the equation for the last $\sim$50 years. For the provision of future sea level trajectories for a reasonable range of forcing scenarios, we will identify the main forcing processes, based on a the analysis of past LSL changes. We will set up a range of forcing scenarios for LSL on the Dutch Coasts using additional information mainly contained in the respective sections of the *Fourth Assessment Report* (AR4) of the *Intergovernmental Panel for Climate Change* (IPCC). Through a weighted combination of these PDFs, we aim to establish an overall LSL PDF for the Dutch coasts.

2 The LSL Equation

LSL is defined here as the distance between the sea surface and the ocean bottom (see Appendix C for details). It is this quantity that is directly related to the potential impact of global and regional changes in climate and sea level in a given area. At any location, LSL is the result of a number of forcing processes acting on a wide range of spatial and temporal scales (see e.g. Chelton & Enfield, 1986; Trupin & Wahr, 1990).

It is worthwhile to mention here that *Global Sea Level* (GSL) change is the spatial integral of LSL changes over the complete ocean area and directly related to the change in the global volume of the ocean. Global averages of sea surface height changes determined by satellite altimetry are not a direct measure of global ocean volume changes and need to be adjusted for changes in ocean floor height (for details, see Appendix C).

For our discussion, it is helpful to separate the LSL equation into a high-frequency and a low-frequency part. For studies of impacts, the combined effects of the high-frequency and low-frequency part of the LSL equation are important. Here we separate these two parts at the period of approximately two months, which is partly motivated by the fact that low-frequency LSL variations are conveniently studied on the basis of monthly mean LSL values.

The high-frequency part can be described by:

$$h_{\mathrm{hf}}(t) = h_{\mathrm{waves}}(t) + h_{\mathrm{tidal}}(t) + h_{\mathrm{atmos}}(t) + h_{\mathrm{seiches}}(t) + h_{\mathrm{tsunami}}(t). \quad (1)$$

where t is time and h is given relative to an arbitrary zero level. The high-frequency part as defined by (1) accounts for waves, tides (up to monthly periods), seiches, tsunamis and atmospherically driven variations on time scales of hours to several weeks. In the following we will focus on the low-frequency part of LSL variations.

The complex interaction between the different processes affecting low-frequency LSL is depicted in Figure 1 on page 13. This figure emphasizes the complex nature of LSL as a parameter resulting from many different

processes. An equation relating these global, regional and local processes to low-frequency LSL variations $h_{\rm lf}$ can be written as:

$$\begin{aligned} h_{\rm lf}(\vec{x},t) &= S(\vec{x},t) + C(\vec{x},t) + A(\vec{x},t) + I(\vec{x},t) + G(\vec{x},t) + \\ & \quad T(\vec{x},t) + P(\vec{x})(t-t_0) + V_0(\vec{x})(t-t_0) + \delta V(\vec{x},t) \end{aligned} \tag{2}$$

where t is time, t_0 an arbitrary time origin, and h is given relative to an arbitrary zero level (Plag, 2006c). As stated above, eq. (2) describes LSL variations on time scales from months to longer. The processes included in eq. (2) are S: steric changes, C: ocean circulation, A: atmospheric forcing, I: mass changes in the large ice sheets, G: mass changes in the continental glaciers, T: mass changes in the terrestrial hydrosphere, P: post-glacial rebound, V_0: secular vertical land motion others than postglacial rebound, δV: non-linear vertical land motion. These processes are discussed in more detail in Table 1 on Page 22 in Appendix B. Similar to Fig. 1, eq. (2) serves well to illustrate the complex nature of LSL variations as the result of processes in the global water and energy cycles merged with geodynamic processes and, recently, anthropogenic activities. As discussed in Table 1, eq. (2) requires detailed models for each individual contribution. For understanding past LSL changes or providing projections of future LSL it is worthwhile to simplify the equation in appropriate ways.

At low frequencies, LSL can also be viewed, in principle, as the sum of four terms: (1) local (steric) changes in the volume of the sea water due to temperature and salinity changes combined with changes in ocean circulation, (2) local changes in the sea surface height due to mass redistribution in the global water cycle including the gravitational effects, (3) vertical motion of the land with respect to the center of mass of the Earth system, (4) changes in LSL due to changing atmospheric forcing (air pressure, wind, evaporation, precipitation and radiation). This leads to a simplified empirical LSL equation of the form

$$h(t) = h_{\rm ocean}(t) + h_{\rm mass} - h_{\rm land} + h_{\rm atmosphere}. \tag{3}$$

This equation is more directly related to observable quantities and well suited to decompose past sea level variations. The LSL h is directly observed by a tide gauge. The steric part of $h_{\rm ocean}$ can be deduced, within certain limitations, from oceanographic measurements of salinity and sea water temperature. It is noted here that the steric contribution includes the effect of freshening of the ocean (Wadhams & Munk, 2004) due to mass added from melting sea ice, glaciers and ice sheets. $h_{\rm land}$ can be measured geodetically in a geocentric reference frame, using, for example, continuous GPS stations co-located with the tide gauges. $h_{\rm atmosphere}$ can be computed by hydrodynamical models driven by the atmospheric forcing or by regression of local meteorological observations on tide gauges records (see Appendix E for details). The only term not directly accessible to observations is the mass term $h_{\rm mass}$. This term combines both a change in the total mass of the ocean as well as a redistribution of mass in the ocean due to changes in the geoid resulting from any mass transport in the Earth system. The relation between mass redistributions in the various reservoirs of the global water cycle and LSL is given by the sea level equation (for details, see Appendix D), which accounts for the effects of the mass redistribution on the gravity field, the shape of the Earth, and Earth rotation, as well as the feedback of Earth's deformations and gravity field changes on the mass distribution in the ocean.

In the absence of specific information on vertical land motion, eq. (3) can be re-written as

$$h(t) = h_{\rm steric}(t) + \tilde{h}_{\rm mass} + h_{\rm atmosphere} - \tilde{h}_{\rm land}, \tag{4}$$

where $\tilde{h}_{\rm mass}$ now includes the deformation induced by mass redistribution in the water cycle, and $\tilde{h}_{\rm land}$ is the vertical land motion due to, for example, tectonics, sediment compaction, or anthropogenic subsidence, but not mass redistribution in the water cycle.

As illustrated in Fig. 1, most of the processes affecting LSL contribute to more than one of the terms in eq. (3). This complicates the interpretation of past LSL variations in terms of causes and, even more so, predicting future LSL variations.

Eq. (3) is well suited for the analysis of past sea level changes. However, for predicting future LSL in response to different specific forcing scenarios, eq. (2) is more appropriate, since each of the processes accounted for in

that equation has its own PDF with specific uncertainties. However, some of the information has to come from the analysis of past observations.

The Dutch coasts is an area where all local, regional and global factors are relevant for the variations and trends in LSL. Moreover, global forcing factors are biased due to the impact of the shallow water depth in the North Sea and the dynamic properties of the English Channel. Consequently, LSL will follow a complex trajectory over time, depending on the specific local mix of the various forcing factors.

3 Past sea level variations

Observations of past LSL changes and relevant forcings can be used to understand and quantify the contributions of steric changes, atmospheric forcing, mass redistribution, and vertical land motion at the Dutch coast. The interval best covered by relevant observations extends from approximately 1960 to present. For that period, both steric observations and meteorological observations are available.

In order to quantify the past LSL trends, we have used the monthly mean LSL data made available by the *Permanent Service for Mean Sea Level* (PSMSL). The PSMSL database is quality controlled (Spencer & Woodworth, 1993; Woodworth & Player, 2003), and for a large number of records, a well documented history of the relation between the tide gauge zero level and the benchmark on land exists. These latter records are those that are referred to as *Revised Local Reference* (RLR) series, while those without a well documented history to a single benchmark are denoted as Metric series. The Dutch tide gauges are referred to a network of benchmarks and therefore the records of these gauges are not included in the RLR data set. However, there is general agreement that these records are of high quality and well suited for studies of low-frequency LSL variations.

The location of all tide gauges with records longer than 20 years are shown in Fig. 2 on page 14 and the start and end years for these records are listed in Table 2 on page 23. It is worthwhile to notice that a number of Dutch gauges have exceptionally long records reaching more than 150 years in one case (Maasluis). Table 2 also includes a set of different estimates of secular trends determined from these records.

For all Dutch tide gauges considered here, LSL trends are positive, indicating a LSL rise over the observation period. The spatial pattern interpolated from the trends is smooth (Fig. 3, upper diagram) with values below 1 mm/yr along the northern coast and values of up to 2.5 mm/yr for the western coast North and South of Hoek van Holland. Comparing the LSL trends obtained for the complete long records (Fig. 3, upper diagram) to trends determined for the interval 1958 to end of record (Fig. 3, lower diagram, see also Table 2), there is a clear indication that average LSL rise over the last century was smaller than for the last five decades (Fig. 3). However, this feature is not necessarily caused by an increase in GSL rise and may be a local or regional feature caused by atmosphere/oceanic interactions.

The large variations in LSL trends on decadal time scale become more obvious in low-pass filtered time series. In Fig. 4 on page 16, the monthly mean LSL records are shown for some of the Dutch and adjacent tide gauges for the intervals 1900-2008 and 1958-2008, after the model given by eq. (11) have been removed and the residuals have been integrated over time. The integration acts as a low-pass filter (Plag, 2000). At these low frequencies, LSL exhibits high spatial coherency particularly if we only look at the last five to six decades (lower diagrams in Fig. 4). For the data before $\sim$1950, spatial coherency is much lower, indicating that data quality may be much less. Therefore, we focus here on the last decades. The low-frequency variations not explained by the model eq. (11) are characterized by variations on time scales of 18 years and 5 to 7 years. The former is most likely due to the nodal tide, while the latter originates from a superposition of the annual and *Fourteen to Sixteen Months Oscillation* (FSO) close to the Pole Tide frequency (see, e.g., Trupin & Wahr, 1990; Plag, 1997; Aoyama et al., 2003, for more details). Moreover, irregular fluctuations at longer time scales are visible, which at most European stations are dominated by a large-scale variation with a typical time scale of $\sim$80 years and a typical amplitude of about 40 mm (Plag, 2000). These fluctuation also cause most of the variations in secular trend estimates obtained from $\sim$5 decades. Because of the large spatial scales, it is likely that most of these fluctuations are caused by atmospheric forcing. In the next section, we will look at the various forcing processes and identify those that are likely contributors to the LSL variations at the Dutch coasts.

4 How have the different processes contributed to past sea-level changes?

For the discussion of the main processes contributing to the observed LSL trends, eq. (3) is utilized. Main focus is on relating the different contributions to observations. A more detailed approach would fill in the numbers for the different terms in eq. (2), but most of these terms are currently rather uncertain.

The effect of the local atmospheric forcing is assessed on the basis of a regression of air pressure and wind stress on LSL (see Appendix E for details). Time series of monthly mean pressure and wind stress for all tide gauges were generated from the pressure and wind field of the ERA40 re-analysis carried out by the *European Center for Medium Range Weather Forecasts* (ECMWF). The results of the regression are summarized in Table 3. The local atmospheric forcing shows a response to air pressure which is coherently below the *Inverted Barometer* (IB) response expected for an equilibrium response to pressure forcing (the regression coefficients are between 33% and 79% of the IB response). The regression coefficients for wind stress components indicate an increase in LSL associated with West and North winds, with the former being by far the dominating wind contributor at most of the Dutch stations.

Fig. 5 shows the contribution of the local atmospheric forcing to the LSL trends in the time window 1958 to 2001. For most parts of the Dutch costs, secular changes in the atmospheric forcing have increased the LSL trends with maximum increases reaching 1 mm/yr in Harlingen, while the atmospheric effect on locations at the English coast and towards the Strait of Dover was to reduce the LSL trends. Similar long-term effects of the atmosphere on LSL are known, for example, for the Adriatic Sea, where a slow increase of air pressure over the last five decades led to a reduction of LSL rise (e.g., Tsimplis et al., 2005). These changes appear to be linked to atmospheric variations on time scales of several decades to centuries as expressed in the long period variations of the *North Atlantic Oscillation* (NAO). In other areas of the world, the impact can be even larger (Plag, 2006e). The feature of a strongly variable effect of the local atmospheric forcing is likely to be the result of long-period oscillations of the coupled atmosphere-ocean system associated with known large scale phenomena. The atmospheric forcing appears to vary on long time scales of five or more decades, and thus can temporarily offset or even reverse a secular rising trend.

After removing the atmospheric effect, the LSL trend pattern still resembles the original pattern over the last five decades (compare the lower diagrams of Figs. 3 and 5), i.e., we see a relatively slow increase at the northern coast and in the Rhine delta, and larger values around Hoek van Holland. Correcting for the atmospheric impact reduces the average LSL rise determined for the period 1958-2001 by 0.5 to 1.0 mm/years. Over a period of five decades, this accumulates to 25 to 50 mm in total mean LSL rise. It can be expected that this impact is of cyclic nature, with a PDF for the total LSL change centered around 0 and realistic 90% boundaries below ± 50 mm[1]. However, if climate change results in a general increase of West and/or North winds, and a permanent shift of the mean air pressure pattern, then a PDF with center value closer to 50 mm and the 90% boundaries adjusted accordingly is more realistic for future LSL changes.

The steric contribution to LSL can be derived from observations of ocean temperature and salinity (e.g., Levitus et al., 2000b,a; Ishii et al., 2003; Levitus et al., 2005). Global models of the steric contribution to LSL variations are available for different data sets and different depth intervals (for example, 500 m, 700 m and 3000 m), and the results obtained by Plag (2006c,e) suggest that all data sets have advantages and deficiencies if applied to global studies. However, for the North Sea, the shallow water depth suggests that the data sets based on the upper 500 to 700 m should be sufficient. Fig. 6 shows the predictions of LSL trends due to steric changes as computed from three data sets of steric LSL variations (Levitus' 500 m and 700 m, and Ishii's 500 m)[2]. The steric contributions to LSL trends are small and do not exceed 0.1 mm/yr along the Dutch coast.

Future changes in GSL due to thermal expansion are estimated to be of the order of 2 to 4 mm/yr, depending on the emission scenario used (Meehl et al., 2007) with a slight increase of the rates towards the end of the 21$^{\mathrm{st}}$. With respect to LSL changes, ensemble studies indicate that the steric effect in the North Sea is likely to be

[1] In absence of a better estimated, the 90% boundaries are estimated as the change we have seen over the last 50 years, taking into account that variations on time scales of $\sim$80 years at European coast have in general amplitudes of about 40 mm (Plag, 2000).

[2] The author is aware that better data sets have become available, however, due to time limitations, these data sets have not been included yet.

larger by ∼0.5 to 1 mm/yr than the GSL rise (see Fig. 10.32 in Meehl et al., 2007). This would be a dramatic increase (by a factor between 30 and 50) with respect to the rates during the last 50 years. However, if we accept these projected changes as maximum values, then a PDF for the steric LSL rise in the southern North could be centered around 2 mm/yr with 90% boundaries at ± 2 mm/yr.

The contribution to LSL trends that is most difficult to assess arises from mass transport in the global water cycle. This contribution is not directly accessible to measurements. It is composed of both an effect resulting from changes in the total mass of the ocean and a redistribution of the ocean mass. The latter is caused by changes in the gravity field associated with mass transport in the Earth system. One contribution results from the viscoelastic response of the Earth to former mass redistributions. The main signal here is due to PGR. Fig. 7 shows predictions for current LSL trends due to PGR for a typical model (the VM2 model, see Peltier, 2004). In the southern North Sea, for this model the PGR signal in LSL is positive along the northern Dutch coast (order 0.6 mm/year) and decreases towards the Strait of Dover where it reaches negative values (order -0.1 mm/year). Most of the signal in the southern North Sea originates from vertical motion of the land, which is dominated by the collapse of the peripheral bulge (subsidence) caused by the former ice loads in Fennoscandia. Model differences are still large (see lower left diagram in Fig. 7), and particularly the exact location of the peripheral bulge is uncertain. Therefore, the PGR predictions need to be associated with uncertainties of the order of ± 0.5 mm/year. For the Dutch coast, a realistic PDF for LSL rise due to PGR has a center value of 0.5 mm/yr and 90% boundaries[3] of ± 0.6 mm/yr.

Concerning LSL variations due to present-day redistributions in the global water cycle, the main sources for mass exchange are the large ice sheet, the continental glaciers, and continental water storage in groundwater, lakes, and reservoirs (Church et al., 2001; Bindoff et al., 2007; Meehl et al., 2007, see Table 5, and). According to the results summarized in Table 5, the total change of ocean mass over the last 40 years is equivalent to approximately -0.41 to 1.09 mm/yr in GSL rise. However, this does not mean that the mass contribution to the LSL trend in the southern North Sea was in the same range. The geoid changes associated with these mass exchanges redistribute the ocean water and result in spatially variable trends (Farrell & Clark, 1976; Mitrovica et al., 2001; Plag & Jüttner, 2001; Plag, 2006c).

For mass changes in the two largest ice sheets, the global LSL fingerprints are shown in Fig. 12 in Appendix D (for details, see there). In the southern North Sea, these fingerprints are nearly constant (Fig. 9). The ratios of LSL change to GSL changes in the southern North Sea are 2.6 ± 0.2 and -2.5 ± 0.5 for the Antarctic and Greenland ice sheets, respectively. Using these ratios and the best estimates of Plag (2006c) for the contribution of the Antarctic and Greenland ice sheet to GSL in the time window 1958-1998[4], we find 0.91 ± 0.65 mm/yr and -0.05 ± 0.04 mm/yr, respectively. These estimates also include the vertical land motion caused by the redistribution of the water and ice loads.

For future changes in ice sheet mass, the contribution to LSL can be computed using the sea level equation (see Appendix D), if the mass changes are sufficiently known. The uncertainties associate with LSL response to mass changes should be small compared to the uncertainties associated with the future trajectory of the ice sheets in terms of mass changes. However, as pointed out in Appendix D, there are still considerable uncertainties with respect to the fingerprints shown in Fig. 9, which could easily be resolved by a rigorous intercomparison of the softwares used to compute these fingerprints. Nevertheless, in particular, the possibility of a largely non-linear response of the ice sheets as discussed, for example, by Zwally et al. (2002); Vaughan et al. (2007) hampers the establishment of reliable PDFs. Moreover, recent studies indicate significant changes in the melting rates of the ice sheets (e.g., Thomas et al., 2004; Tedesco, 2007) and also the sea ice (Stroeve et al., 2008), with the latter potentially leading to a more rapid freshening of the ocean (Wadhams & Munk, 2004). Assuming that the contribution from non-linear events will be limited over the next one to two centuries, then temperature sensitivities of the two ice sheets as established by model studies can be used to get an estimate of the ice sheet contributions as function of future temperature changes. However, the sensitivities given by Meehl et al. (2007) are for temperature changes over the ice sheet, not for global temperature changes (see table 10.6 in Meehl et al., 2007). Therefore, a reasonable approach could be to take the estimates of the ice sheet

[3]These boundaries are estimated from an set of twelve different PGR model predictions.

[4]These estimates are well in the range given for these ice sheets in Bindoff et al. (2007)

contributions as given in Table 10.7 of Meehl et al. (2007) and use these together with the fingerprint functions for the ice sheets to estimate the likely contribution at the Dutch coast. Alternatively, the ice sheet contributions as estimated by Meier et al. (2007) can be adopted. In addition, extreme melting events could be considered.

Past contribution of mountain glaciers are estimated by Meier & Dyurgerov (2002) to be $\sim$0.4 mm/yr for the interval 1960 - 1990 (see Table 5). Estimates of the rates resulting from changes in land water storage (excluding glaciers and ice sheets) are in the range from -1.1 mm/yr to 0.4 mm/yr (see Table 5). In the absence of better estimates or a detailed model of the mass redistribution, we have to assume these values for the Dutch coast. However, it is pointed out here that estimates for current contributions of the ice sheets are much higher (Meier et al., 2007), and of the order of 1.1 ± 0.24 mm/yr. We will therefore use the values given in Table 1 in Meier et al. (2007) for 2050 and 2100 for scenarios and predictions.

For the LSL equation, vertical land motion needs to be given with respect to the *Center of Mass* (CM) of the complete Earth system including solid Earth, ocean and atmosphere. However, most of the observational evidence of vertical land motion on time scales longer than a few years is relative. Currently, continuous GPS (CGPS) is the only logistically viable technique allowing for the determination of vertical point motion with respect to the CM, though still with a limited accuracy. Unfortunately, even the longest GPS records cover only about 15 years. Therefore, vertical velocities determined from these records are representative for a short time window only, and it is not obvious that these rates can be considered to be the same as the secular velocities.

The Nevada Geodetic Laboratory includes a number of CGPS stations around the North Sea in operational daily analyses (Fig. 11). Selected time series have been analysed by fitting eq. (11) to the time series of daily vertical displacements. The results are summarized in Table 4. The CGPS sites at the northern Dutch coast appear to be subsiding while those further south and at the English coast are uplifting with the largest uplift found for Sheerness. The subsidence of the northern Dutch coast is in agreement with the prediction of most PGR models (see Fig. 7, upper right diagram). An uplift of the coast from Delft towards south and around the Strait of Dover is not predicted by the PGR models but could still be partly due to PGR. However, the spatial pattern of vertical land motion with subsidence on the northern coast and uplift towards the English Channel is not anti-correlate with the spatial pattern of LSL rise (Fig. 3)[5]. Both the original LSL trend pattern and the trend pattern after atmospheric impact has been removed are positively correlated with the spatial pattern in vertical land motion. The reason for this significant mismatch between expected and observed relation of secular vertical land motion and LSL changes is not clear.

In order to assess how well we can explain the observed LSL trends for the individual tide gauges, we define the LSL balance as

$$\delta b = b_{\mathrm{observed}} - b_{\mathrm{atmosphere}} - b_{\mathrm{steric}} - -b_{\mathrm{PGR}} - b_{\mathrm{Antarctica}} - b_{\mathrm{Greenland}}. \tag{5}$$

δb accounts for all contributions not explicitly included in this equation, including changes in glaciers, ice caps, and other terrestrial water storage, as well as vertical land motion due to tectonics, sediment compaction, or anthropogenic processes. For the tide gauge BOR, $\delta b = 2.50$ mm/yr (Table 6) indicates significant local subsidence. This subsidence is confirmed by the GPS results for the CGPS site BORJ (Table 4), which is very close to the tide gauge BOR. All other gauges at the northern Dutch and adjacent German coasts have negative balances. Partly, this could be due to an overestimation of the PGR signal, which associates this region with the subsiding peripheral bulge. For the gauges HOE, MAA, and STE, the balance is between 0.59 and 1.59, possibly indicating that this area is subsiding. However, the two CGPS sites in this area (DELF and DLFT) indicate land uplift. The abnormal balance for tide gauge CAL is most likely due to problems in the tide gauge record and not further discussed. The small LSL trend at SOU is also likely to be the result of problems in the benchmark history of this record. All other tide gauges at the Belgium and English coasts have positive balances, which would be consistent with subsidence, while the CGPS sites indicate land uplift. A potential cause of this discrepancy may be in the PGR model predictions. The mass contribution from glaciers, ice caps, and other components of the terrestrial hydrosphere are unlikely to produce a pattern with small spatial

[5]We would expect that LSL shows an inverted spatial pattern with respect to vertical land motion, with subsidence associated with larger LSL trends and uplift with smaller trends

scales. However, anthropogenic processes (in particular water table changes caused by groundwater mining or irrigation, or oil extraction) may cause some of the small scale variations.

For sea level projections as a basis for the planning of adaptation and mitigation, considering the secular trend is only a part of the picture. The other part comes from changes in the statistics of sea levels exceeding a given threshold and thus causing flooding. For a stationary mean LSL, the statistics of these events are mainly determined by the statistics of storm surges. For an increasing LSL, the tides also contribute to changes in the statistics of extreme LSL values (Marbaix & Nicholls, 2007).

5 Probability density function

A key question is whether there is a global relationship between the PDF for global temperature and a PDF for GSL rise. Even if such a relationship could be determined for the past based on a GSL sensitivity to global average temperature, then it has to be doubted that this relationship also would apply to the future. Both LSL and GSL are the result of many processes with different spatial and temporal scales. An empirically determined relationship between PDFs for global temperature and GSL would only be applicable to the future if the mix of processes contributing to GSL would be the same in the future as it was in the past. However, this is highly unlikely. Therefore, an experimentally determined PDF for GSL as function of the PDF for global temperature cannot be extrapolated into the future. However, one might consider to establish the temperature to GSL PDF relationship based on model studies. This would be possible if the models capture all relevant processes accurately enough.

If such a PDF for GSL could be established, it would, however, not be very helpful for local or regional studies. One purpose of the previous two sections was to show that the individual processes are associated with their specific spatial fingerprints and their spatially variable PDFs. Therefore, only a detailed local study can lead to reasonable PDFs for the individual processes and a combined PDF allowing to construct likely future trajectories of the LSL.

In Table 7 we have summarized the PDFs established in the previous Section. These PDFs can be used to set up LSL predictions for a plausible range of forcing scenarios over 50, 100 and more years.

In order to elucidate the uncertainties in forcing scenarios and predictions of future sea levels, a set of possible forcing scenarios for the future LSL at 2050, 2100, and 2100 is synthesized from a combination of the various processes contributing to LSL at the Dutch coasts. A simple, precautionary approach proposed by Hulme et al. (2002) would take the GSL scenarios provided in the Fourth Assessment Report (FAR) of IPCC and multiply them by 1.5 in order to account for potential local to regional amplifications. However, this approach might easily lead to estimates far too large since it is not allowing for the spatial variability of all the relevant sub-global processes. In general, this is true for any coastal location, due to the spatially highly variable fingerprints of all forcing factors on sea level. For the Dutch coasts, it is even more so due to the location in the southern North Sea and the vicinity to the English Channel and particularly the Strait of Dover, which biases all forcing coming from the Atlantic Ocean, as well as the difficulties encountered in the interpretation of past contributions. Based on the understanding of the past sea-level changes in the southern North Sea and realistic estimates for the future contribution of thermal expansion (Meehl et al., 2007) and the cryosphere (Meier et al., 2007), we determined a set of plausible LSL projections, taking into account the considerable uncertainties (Table 8). The set of plausible projections of mean LSL changes for the Dutch coasts considered here turns out to cover a wide range of possible sea levels for the three points in time chosen. The projections range from -33 to 358 mm in 2050, -346 to 856 mm in 2100, and 358 to 1158 mm in 2200. The uncertainties in the individual projections are large and of the order of 150 mm, 300 mm, and 500 mm for 2050, 2100, and 2200, respectively.

Main uncertainties result not only from the contribution of global processes (ice-sheet melting and ocean warming) but also from local contributions such as local vertical land motion, changes in the local meteorology and regional processes in the North Sea. In a world with more or less linear extrapolations of todays's rates superimposed by expected climate impact, the single most important uncertainty is associated with the steric contribution resulting from thermal expansion. For the scenarios with accelerated melting of ice provided by

Meier et al. (2007), the uncertainties for the individual contributions of the ice sheets and glaciers are all of the same order as the uncertainties of the steric contribution and combined determine the overall uncertainties. For the vertical land motion, the main uncertainty is attributed to the relation of the origin of the global geodetic reference frame to the center of mass of the Earth system (Plag et al., 2007).

The scenarios and projections compiled in Table 8 do not account for catastrophic disintegration of the Greenland ice sheet or the West Antarctic ice sheet. While the former most likely would result in a net reduction of LSL at the Dutch coast, the latter would lead to a very large LSL rise, depending on the amount of ice melted.

6 Conclusions

The analysis of the past LSL changes along the coasts of the southern North Sea shows that most of the observed LSL variations can be explained by a contribution from PGR, changes in atmospheric forcing, steric changes, and the melting of the Antarctic and Greenland ice sheets. However, a spatially variable discrepancy between observed and synthezised LSL trends could be indicating that the PGR model used is misplacing the peripheral bulge.

Based on the analysis of the past LSL variability and the predictions for future contributions of the cryosphere, PDFs for the individual forcing processes could be established. Some of these PDFs are associated with large uncertainties, which propagate into LSL scenarios and projections. A major result of the present study is the large range of plausible future sea-level trajectories in the 21^{st} century and their uncertainties. These uncertainties, which are confirmed in other, similar studies, need to be considered as an integral part of the plausible futures.

7 Comments on the Five Questions

1. Can a probability density functions (PDFs) of future global temperature changes be translated into PDFs of the global sea level rise for the year 2050, 2100, 2200? *The fact that a number of processes contribute to both GSL and LSL changes with each process being associated with a very specific dependency on global, regional or even local temperature prohibits an approach linking a PDF for GSL directly to a PDF of global temperature changes. Even if this relation could be established for a certain time interval, there is no guarantee that a similar relation holds for other time windows.*

2. If it is too difficult to construct the above mentioned PDFs, could the author give a best personal scientific judgement about the mean $\mu = X_2$ and the means of the extreme values X_1, and X_3, the lower and upper bound respectively (see the Figure below) for the year 2050, 2100, 2200? (still referring to global sea level rise)? *Resonable estimates of GSL in 2100 are actually given in Table 10.7 in Meehl et al. (2007).*

3. Can the full range of possible futures regarding the effect of melting of the Greenland and Antarctic ice sheets on the global sea level be explicitly be stated? Can this be expressed in terms of mean value and extremes as in the previous question? *The more or less linear response included in current models is already fairly well known. The big uncertainty is in dynamic, non-linear responses. Although there is only a principle limit due to the energy needed to actually melt the ice, I don't think it is realistic to assume the most dramatic event. However, changes in GSL caused by ice sheet melting on the order of 1 to 2 m over 100 to 200 years can hardly be excluded. Considering that we have entered the Anthropocene, and, as demonstrated by, for example, Turner II et al. (1990), have changed the Earth system dramatically, even the fact that rates close to 2 m/century have not been observed in the past does not exclude that such rates cannot occur under the current conditions.*

4. At regional level, how will climate change and sea level rise affect the mean sea levels in the North Sea in the year 2050, 2100, 2200? *The answer to this question is given in Table 8. The projections compiled in this Table are based on the PDFs of the individual processes as given in Table 7.*

5. What are the author's argued views about the effect of global warming on the maximum wind velocity, storm surge levels and wave heights and what about the possible changes in the (the for set up along the Netherlands shores) most relevant wind directions during extreme storms in the North sea area? *I have not considered this question.*

A Figures

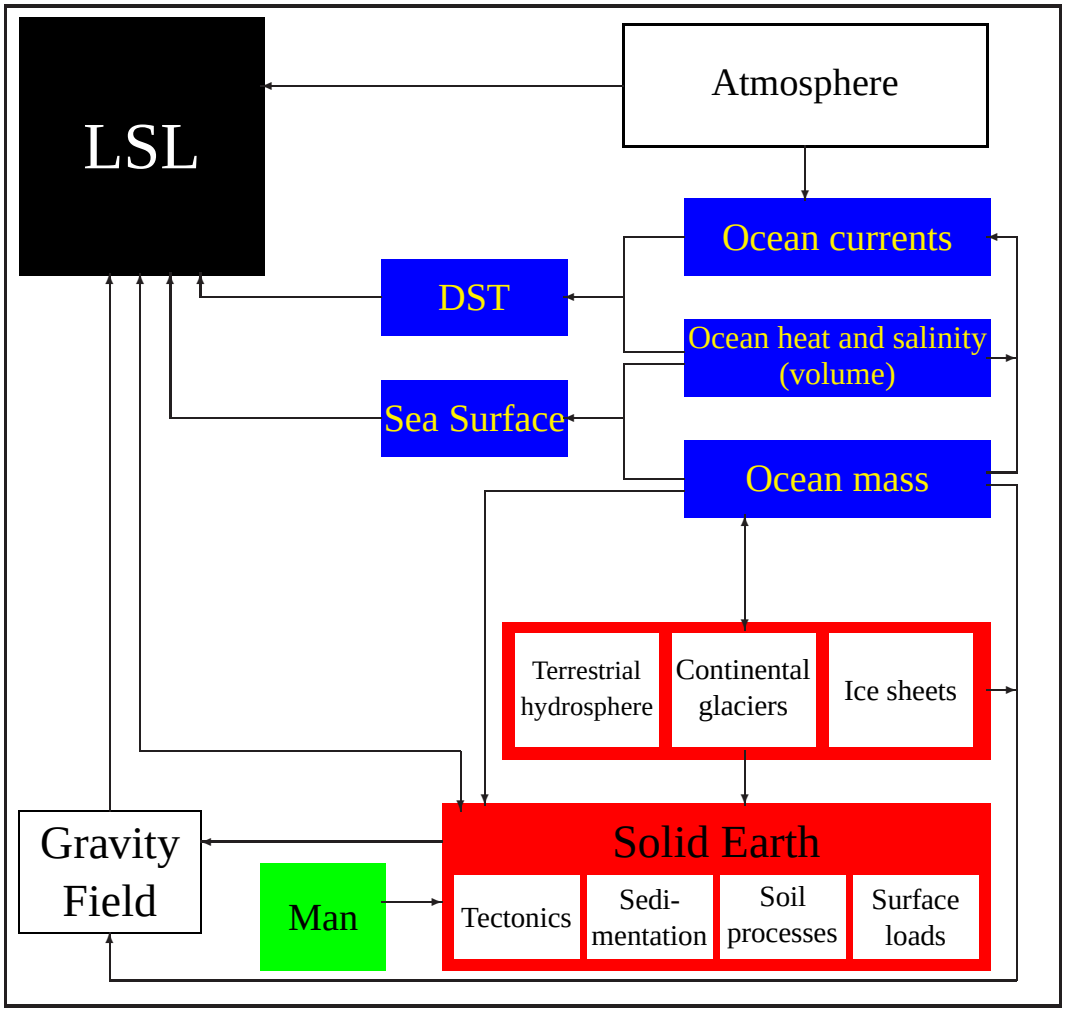

Figure 1. Interaction of processes controlling LSL. Mass movements in the terrestrial hydrosphere (groundwater, rivers, lakes, and reservoirs) and land-based cryosphere (glaciers and ice sheets) and mass exchange with the ocean load and deform the solid Earth and affect the gravity field. The deformations and the associated gravitational changes result in LSL changes, depending on where mass has been relocated. Ocean mass changes change the sea surface position, similar to ocean volume changes caused by heat and salinity changes. Mass and heat changes also affect the ocean currents and thus change the *Dynamic Sea Surface Topography* (DST). Atmospheric circulation forces wind-driven currents, which also influence the DST. DST and sea surface changes caused by regional and global processes change LSL in any location. The atmosphere also acts locally on the sea surface and thus changes LSL. Past changes in the ice sheets and glaciers lead to PGR, which affects LSL through vertical land motion and geoid changes. Tectonic processes in the solid Earth both result in vertical land motion, changes in the size of the ocean basins, and changes in the geoid. In areas where sedimentation takes place, the compaction of the sediments and their load on the solid Earth introduce vertical land motion. Moreover, changes in LSL feed back on the solid Earth and can cause the destruction of peat through oxidation and thus lead to subsidence. Finally, anthropogenic vertical land motion associated with exploitation of groundwater, oil and gas can change the Earth's surface position. Variations in sedimentation due to river regulation (reduction) or land use (increase) also affect LSL particularly in the vicinity of river deltas. For any given coastal location, all these interacting processes need to be assessed in order to understand past sea-level changes and to set up forcing scenarios and determined projections of future LSL changes. From Plag (2006b).

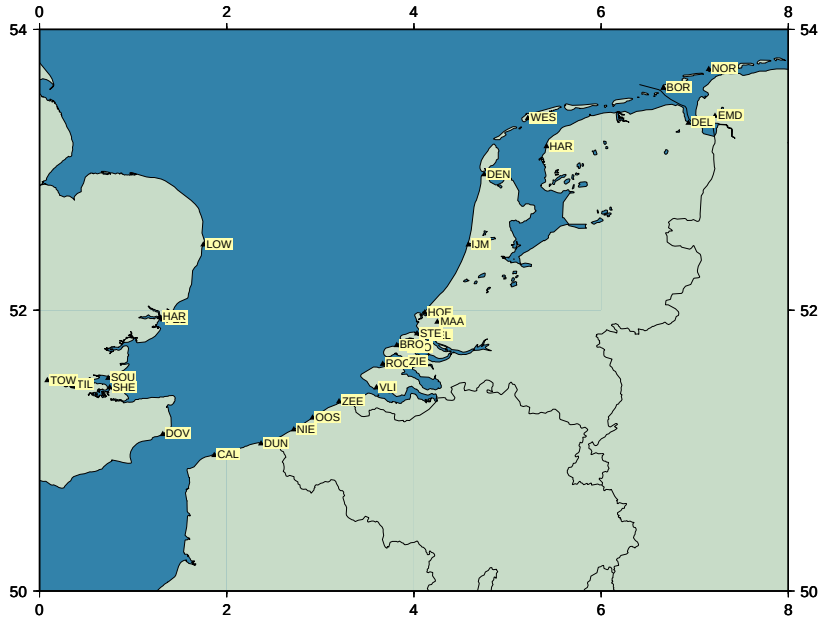

Figure 2. Tide gauge locations at the Dutch and adjacent coasts. Tide gauge locations are taken from the PSMSL data base. Full station names are given in Table 2 on page 23.

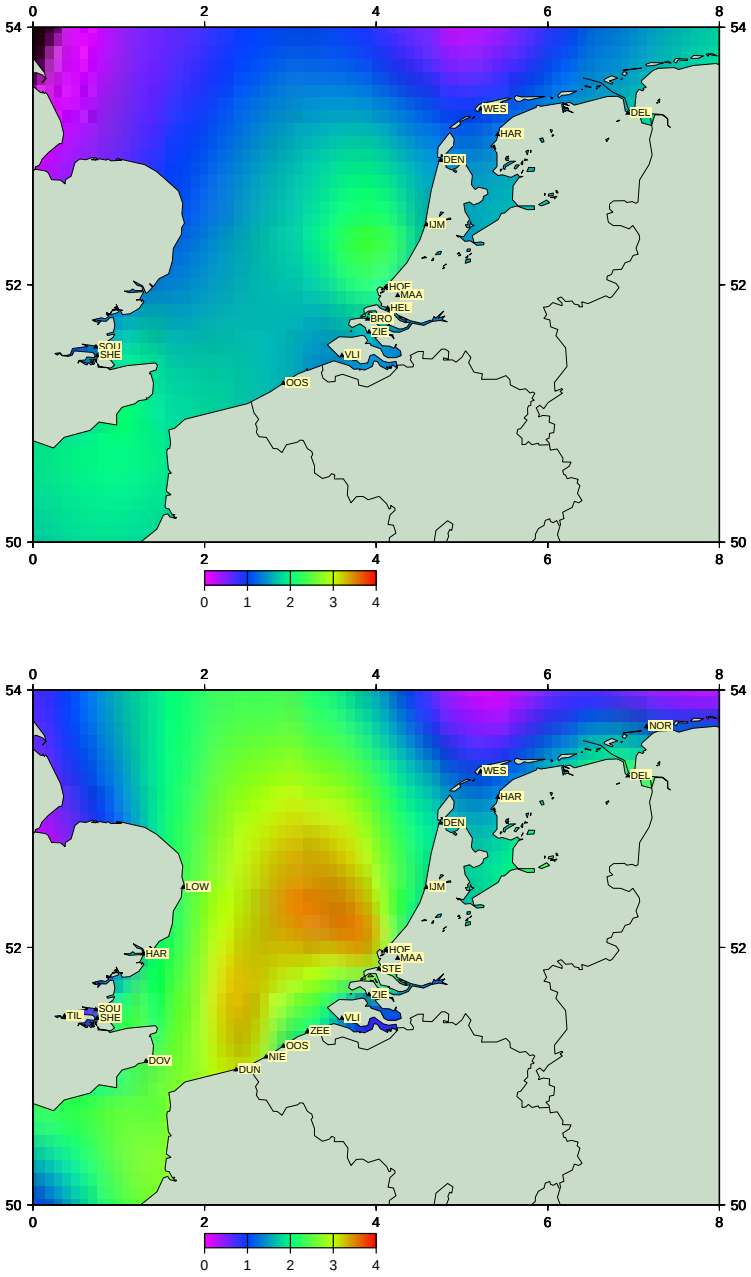

Figure 3. LSL trend pattern in the southern North Sea and part of the English Channel. Trends are in mm/yr. Left: Trend pattern interpolated from long records with all data used in the interval 1840 to 2008. See Table 2 for details on the record. Right: same as left but for trends determined in the interval 1950 to 2008. The tide gauges used for each of the diagrams are shown.

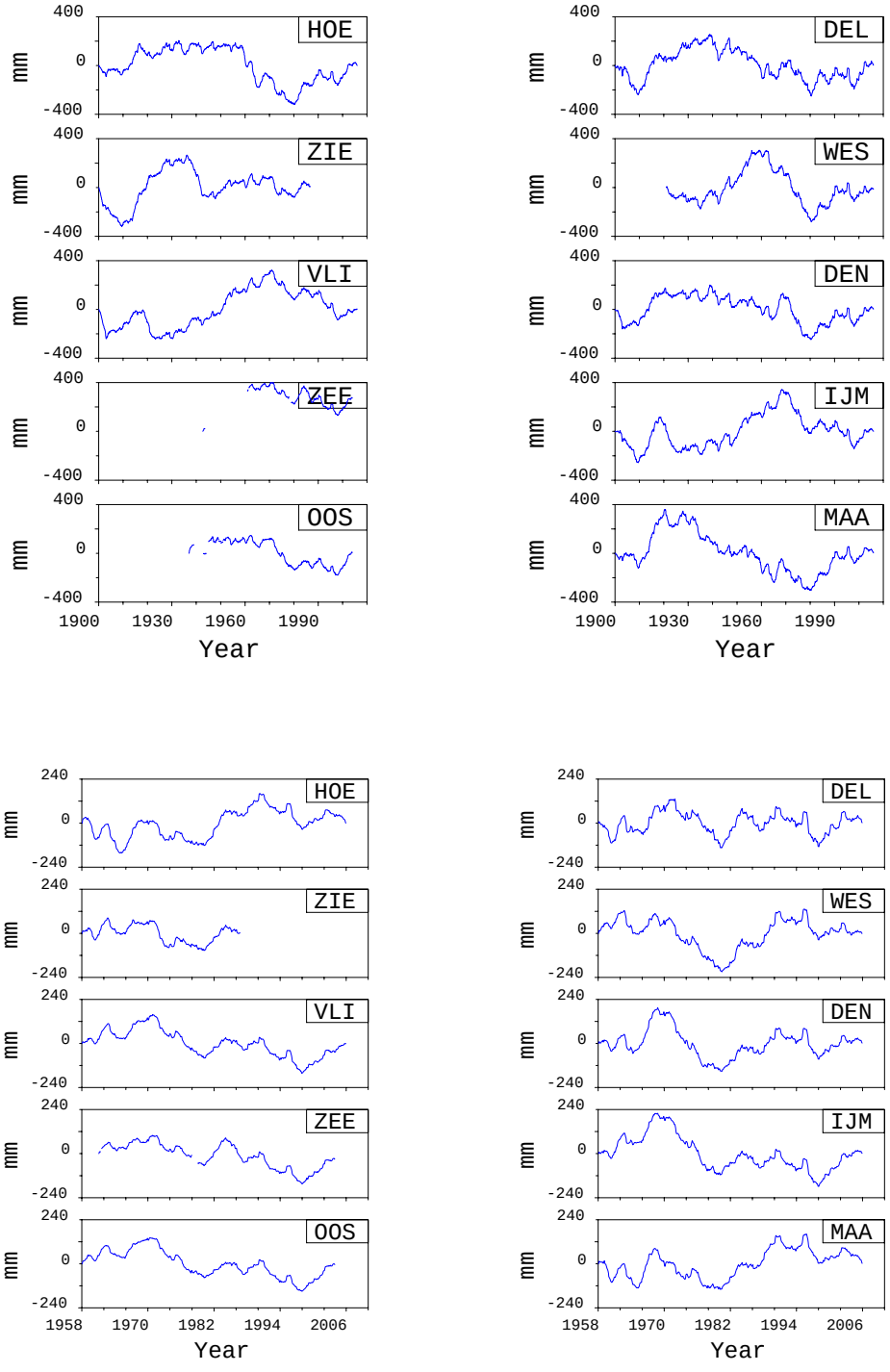

Figure 4. Integrated residual sea-level records. Shown are the integrated residuals with respect to the modeled $h(t)$ as described by eq (12). The residual time series are integrated using $\hat{h}(t) = \int_{t_0}^{t} R(t')dt'$, where R is the residual. Methodology is from Plag (2000). Station abbreviations are as given in Table 2. Upper two diagrams: Time window 1990 - 2008. Lower two diagrams: Time window 1958 to 2008.

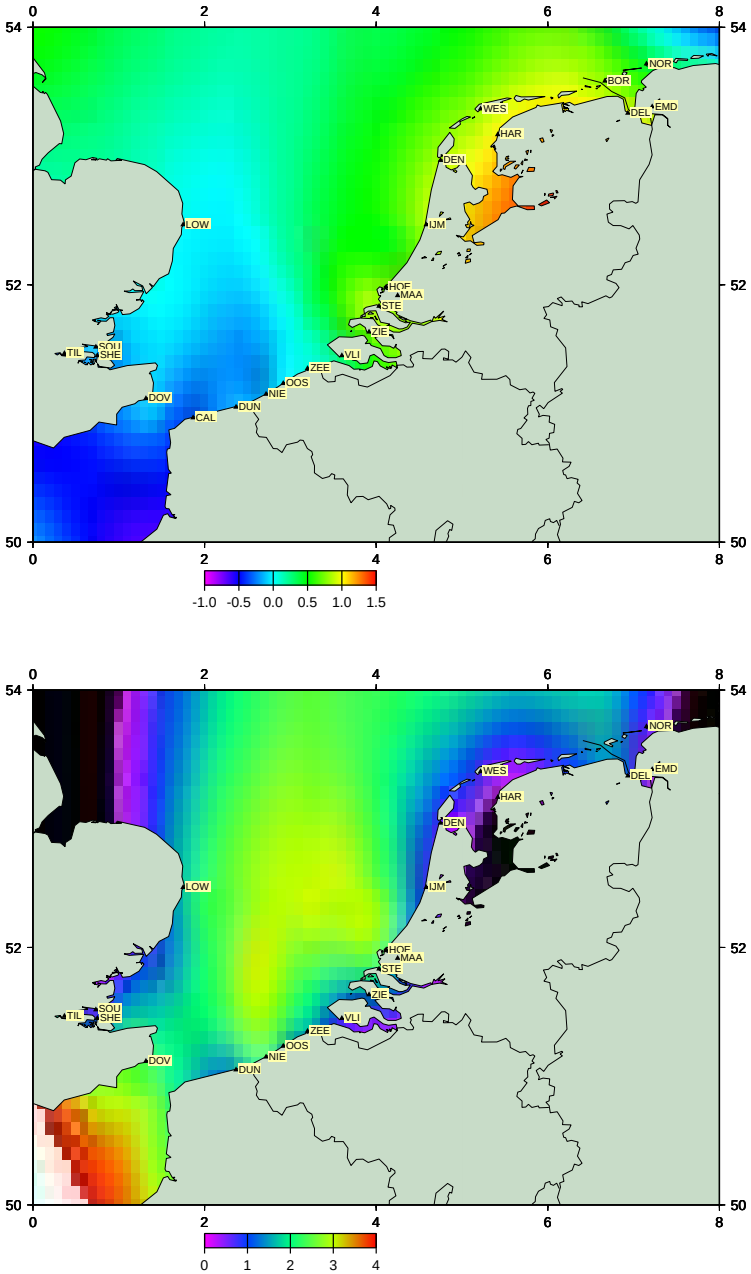

Figure 5. Spatial pattern of the impact of atmospheric forcing on LSL trends. For details on the records see Table 2. Trends are in mm/yr. Upper diagram: The collective impact of atmospheric forcing at a tide gauges is determined as the difference $b_1 - b_2$ of the secular sea level trends b determined in a regression without (eq. (11)) and with (eq.(12)) atmospheric forcing, respectively. The patterns have been interpolated from the tide gauges as indicated. Lower diagram: LSL trend after local atmospheric impact has been removed. Note that Calais and Bordesholm were not included because of their LSL trends (see Table 2) indicating significant local effects. Note that the interpolated values at the corners of the diagrams are highly uncertain.

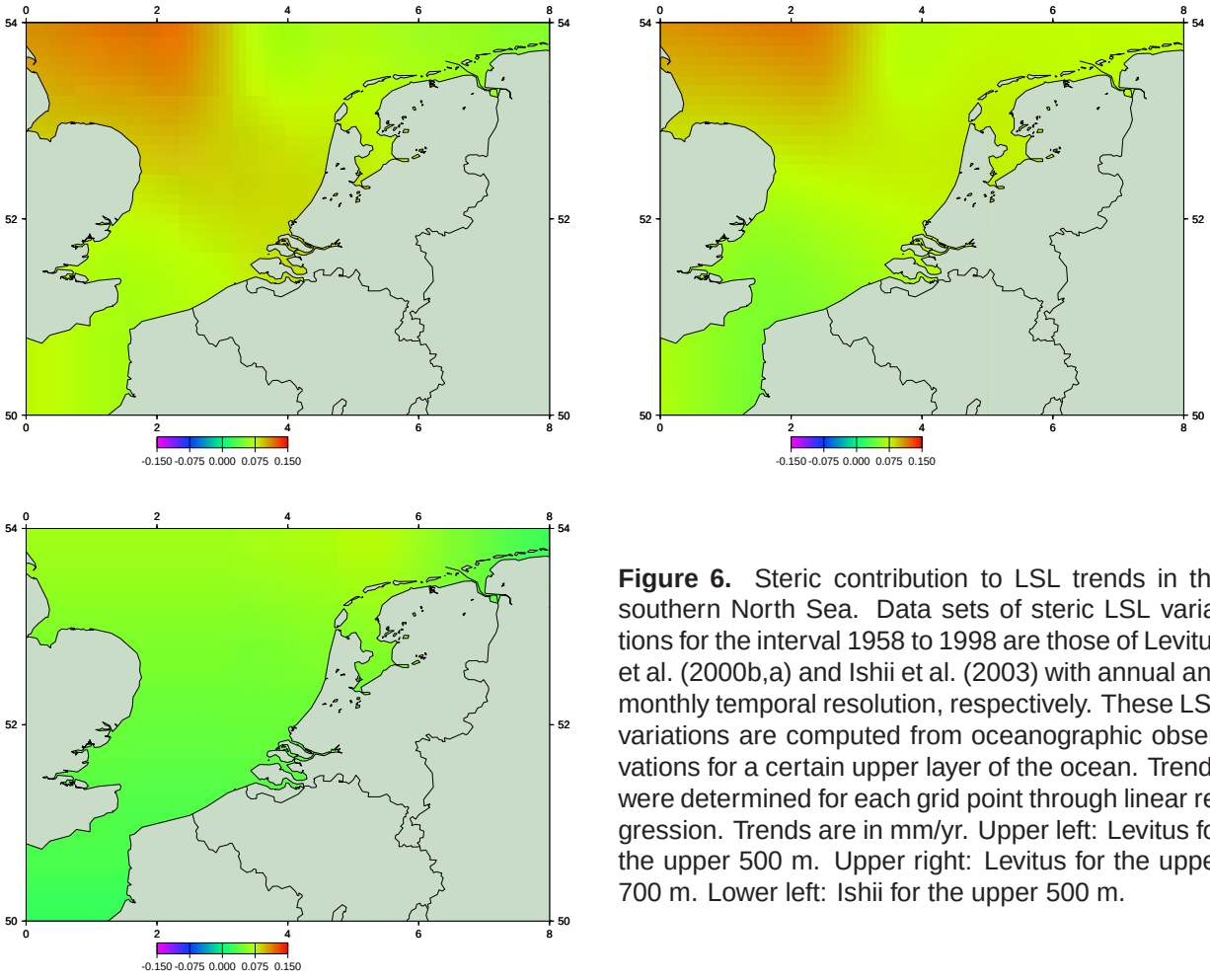

Figure 6. Steric contribution to LSL trends in the southern North Sea. Data sets of steric LSL variations for the interval 1958 to 1998 are those of Levitus et al. (2000b,a) and Ishii et al. (2003) with annual and monthly temporal resolution, respectively. These LSL variations are computed from oceanographic observations for a certain upper layer of the ocean. Trends were determined for each grid point through linear regression. Trends are in mm/yr. Upper left: Levitus for the upper 500 m. Upper right: Levitus for the upper 700 m. Lower left: Ishii for the upper 500 m.

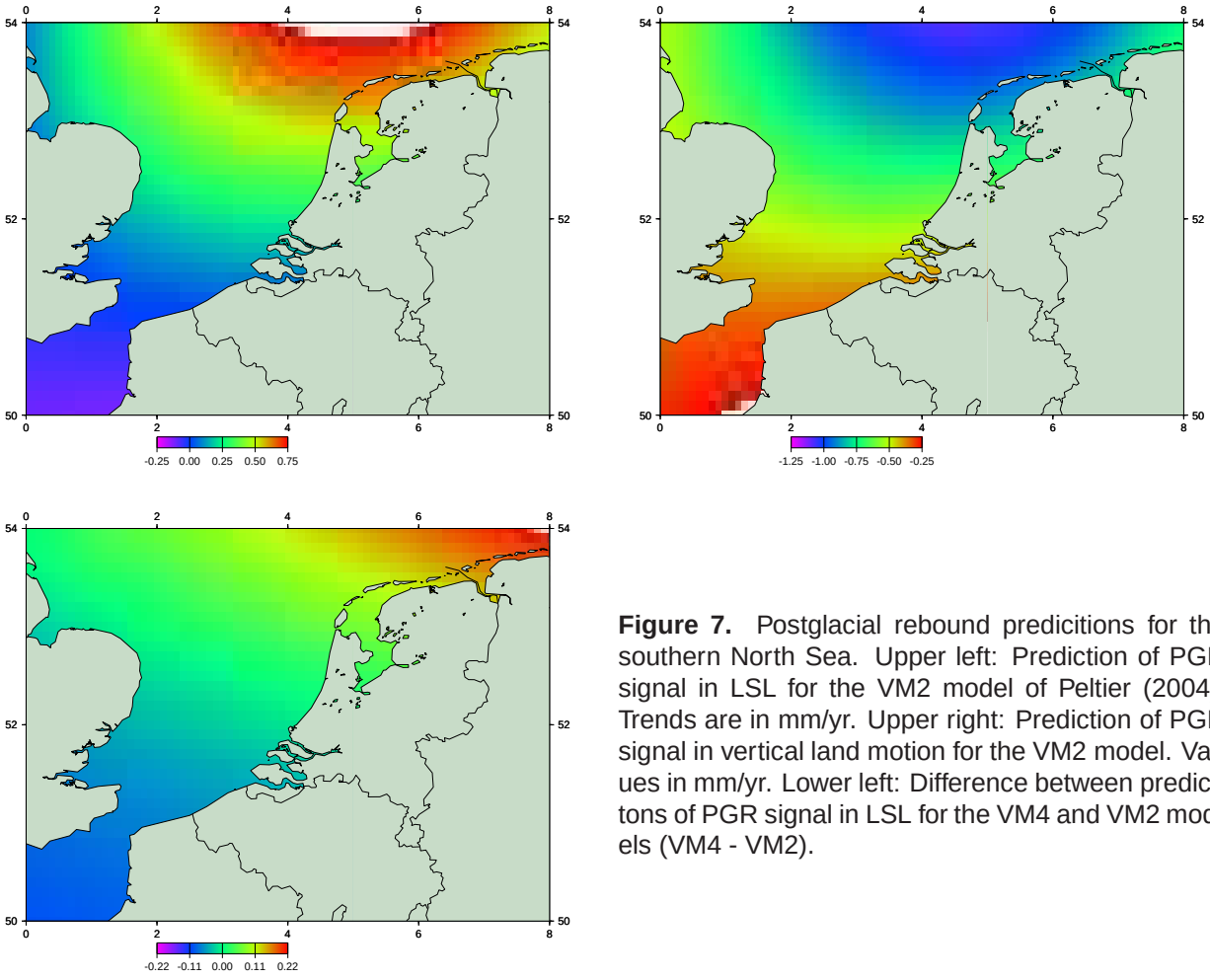

Figure 7. Postglacial rebound predicitions for the southern North Sea. Upper left: Prediction of PGR signal in LSL for the VM2 model of Peltier (2004). Trends are in mm/yr. Upper right: Prediction of PGR signal in vertical land motion for the VM2 model. Values in mm/yr. Lower left: Difference between predicitons of PGR signal in LSL for the VM4 and VM2 models (VM4 - VM2).

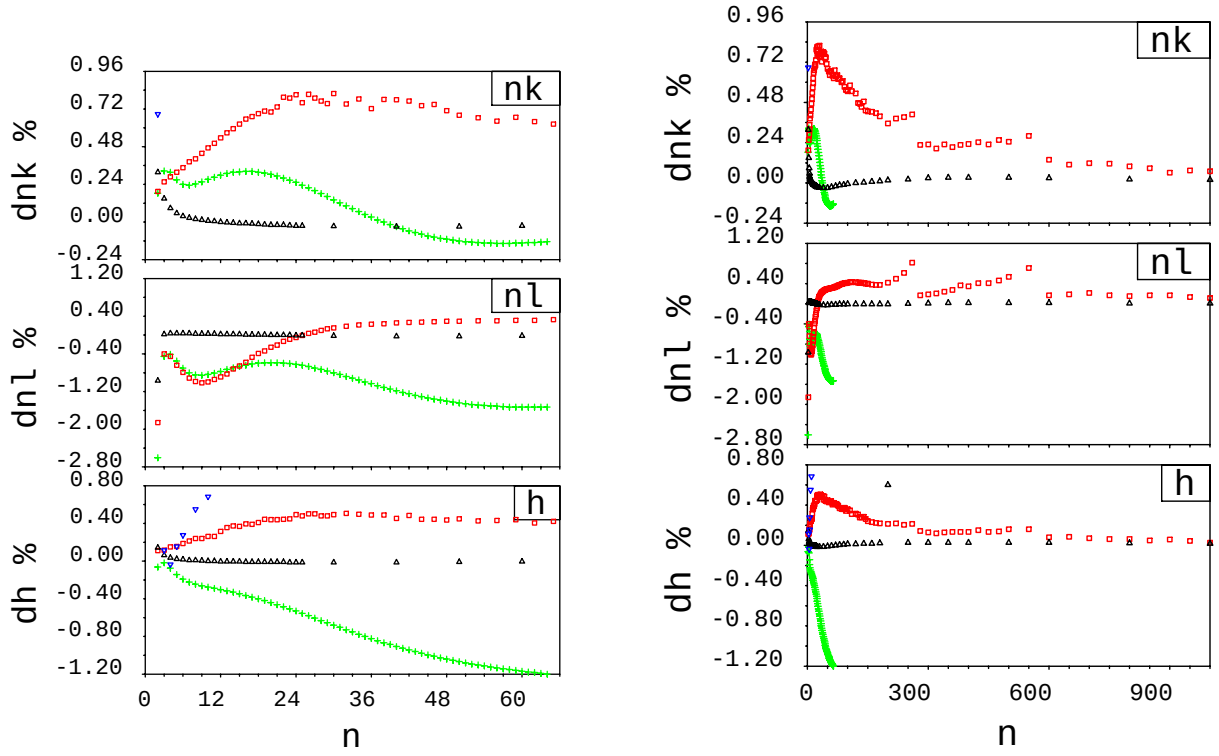

Figure 8. Load Love Numbers computed by different groups. The quantities shown are relative deviations from the LLN provided by Gegout (2003), i.e., for example, $\frac{h_n^{(\mathrm{X})} - h_n^{(\mathrm{PG})}}{h_n^{(\mathrm{PG})}}$ and similar for the other LLNs. Green crosses are for Tamisiea et al. (2003), red squares are Plag (1998), and black triangles Francis (2003). All LLNs are for the Earth model PREM. Note that only for Plag (2003), $h_0 \neq 0$ as expected for a compressible Earth model. The LLNs provided by Farrell (1972), which are still widely used for load calculations, are for a Gutenberg-Bullen model and deviate up to 20% from the LLNs for PREM.

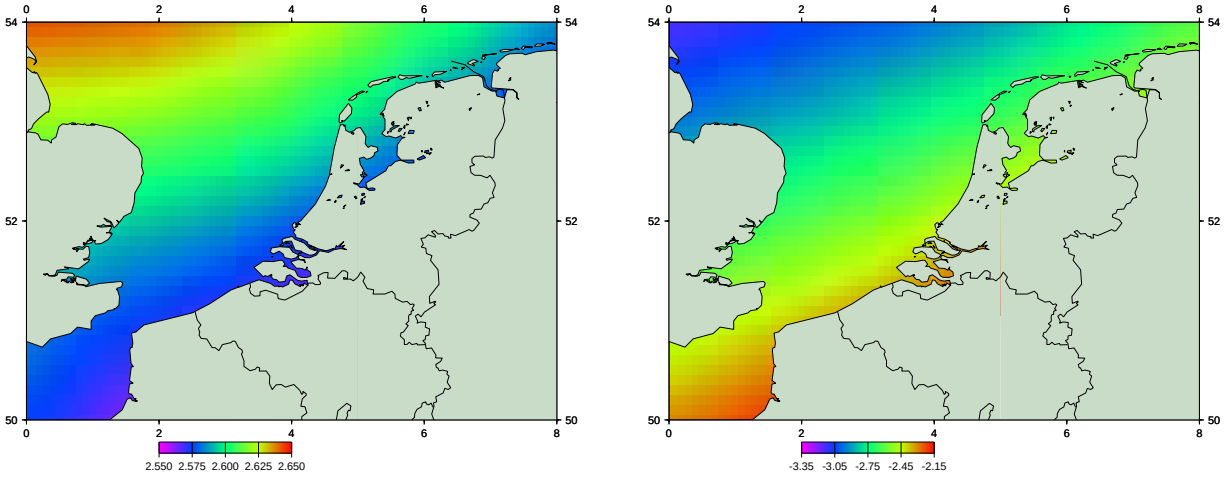

Figure 9. LSL fingerprints of mass changes in ice sheets for the southern North Sea. Shown are the LSL changes relative to GSL changes for a uniform change of the Antarctic (left) and Greenland (right) ice sheets. For a known GSL contributions, the mean factors of 2.6 and -2.75 for Antarctica and Greenland can be be used to compute the contribution to LSL at the Durch coasts. For more details on the computation of the fingerprints, see Appendix D.

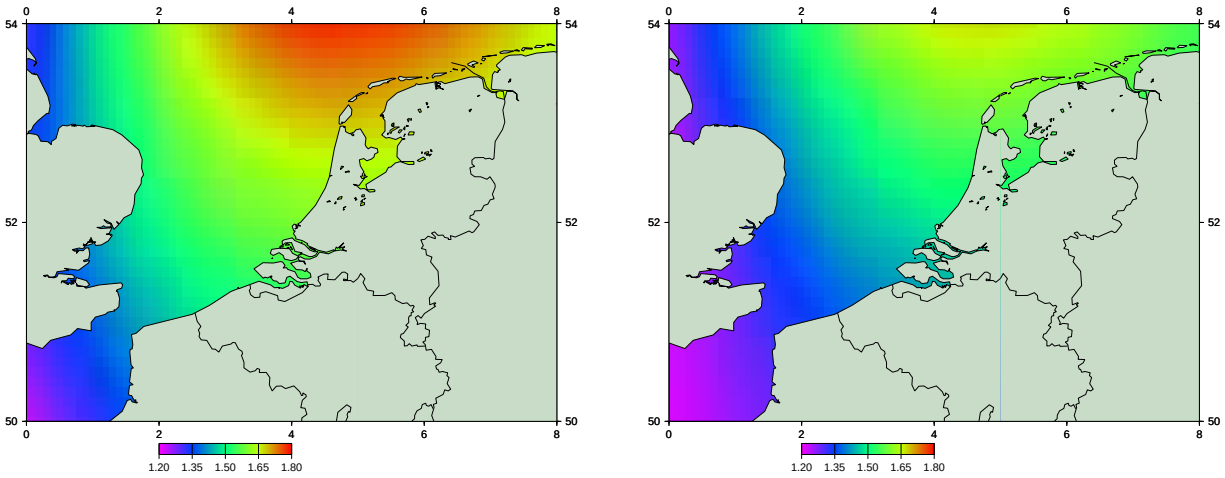

Figure 10. Predictions of global LSL models for the southern North Sea. The models are those shown in Fig. 5 in Plag (2006c). The forcing factors accounted for are Antarctica, Greenland, PGR, steric changes, and a globally constant contributions. For the steric contribution, the Levitus 500 m (left diagram) and Ishii 500 m (right diagram) data sets were used. On average, the model predictions are close to the observed sea level changes, but they do not reproduce the lower values of LSL rise at the northern Dutch coast.

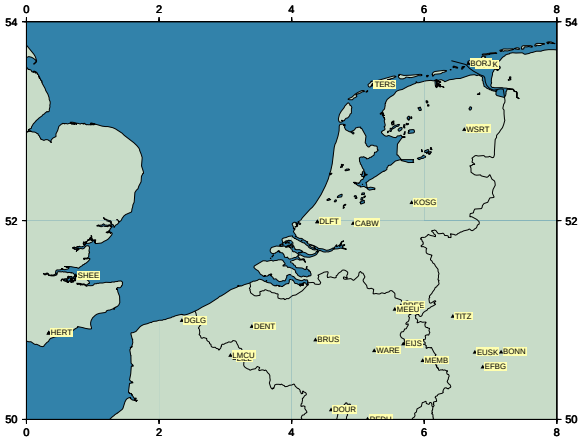

Figure 11. Location of CGPS site. Locations shown are for those sites routinely processed at the Nevada Geodetic Laboratory. Note that DLFT has the same location as DELF. The location of BORK is very close to BORJ.

B Tables

Table 1. Processes affecting LSL and information sources.

V.	Process	Past sea levels	Future scenarios
T:	Long period tides:	Besides components with shorter periods, the astronomical tidal potential also contains constituents in the fortnightly, monthly, semi-annual and annual frequency bands (e.g. Cartwright & Edden, 1973; Tamura, 1987). Moreover, the nodal tide adds a long-period tide with a period of 18.6 years. The fortnightly and monthly tides, which are at the maximum of the order of a few centimeters, are greatly reduced in the monthly LSL records. The semi-annual and annual astronomical tides as well as the nodal tide are small (of the order of 5 to 10 mm) compared to the sea level variations induced by climatological forcing.	
S:	Local steric forcing:	The past local steric forcing can be derived from observations of ocean temperature and salinity (e.g. Levitus et al., 2000b,a; Ishii et al., 2003; Levitus et al., 2005). There are new improved temperature and salinity data sets available, which should be considered. Global models of S are available for different data sets and different depth intervals (namely 500 m, 700 m and 3000 m), and the results obtained with our previous model suggest that all data sets have advantages and deficiencies (Plag, 2006c,e). Particular attention has to be on the uncertainty introduced by the extrapolation of S to tide gauge and coastal locations.	Future scenarios have to rely on results from model runs, in particular ensemble studies that help to characterize the PDF for S.
C:	Ocean circulation changes:	Most of the LSL changes associated with circulation changes are already taken into account thorugh the steric changes (Meehl et al., 2007). Therefore, particular attention has to be on avoiding "double counting".	
F:	Sea ice changes:	The computation of the effect of sea ice melting and the freshening of the ocean (Wadhams & Munk, 2004) can be based on a global inventory of sea ice for the last 50 to 100 years. Such inventories are available from several sources, such as the National Snow and Ice Data Center. However, it has to be assess to what extent the effect of freshening is already included in the observed steric changes. In any case, the effect of the density difference between ice and sea water will have to be included.	
A:	Local atmospheric forcing:	The atmospheric forcing contains a wide range of climatological variations at intraseasonal and seasonal time scales up to phenomena such as the *North Atlantic Oscillation* (NAO) (see e.g. Hurrell, 1995; Hurrell & van Loon, 1997), the *Northern Hemisphere Annular Mode* (NAM) (Thompson & Wallace, 2001), and the *El Niño/Southern Oscillation* (ENSO) (see e.g. Philander, 1990) with typical periods of several years to decades. Oscillations in the climate system with periods of several decades to a century as described by e.g. Schlesinger & Ramankutty (1994) may also be associated with long-period variations in sea level captured by tide gauge records (e.g. Plag, 2000). For past sea level changes, the effect can be estimated using regression (Plag, 2006e). Alternatively, the atmospheric contribution could be derived from a hydrodynamic model. This approach, which is extremely demanding in computational resources, was used e.g. by Tsimplis et al. (2005) for the Mediterranean. However, a comparison of the LSL variations predicted by the hydrodynamical model to those resulting from our approach for the Adriatic showed that the differences are of the order of 5% (Plag, 2006, unpublished study). Nevertheless, if a global prediction from a hydrodynamical model becomes available (plans for a global model run based on the ERA40 data set are currently under discussion in two European groups), then these model outputs would be a good independent estimate of the atmospheric effect.	
I:	Contribution of large ice sheets:	The mass changes of the large ice sheets are poorly known (see the discussion in Church et al., 2001; Bindoff et al., 2007). Therefore, we will use the results of Plag (2006a) together with the fingerprint approach (Plag & Jüttner, 2001; Mitrovica et al., 2001). For a unit change in the mass of a given ice sheet, the LSL fingerprint can be computed from eq. (10). As justified in the text, we use only the elastic, instantaneous part of this equation. Plag & Jüttner (2001) and Plag (2006c) discuss that the tide gauge network is not sensitive to the exact location of mass sources within the large ice sheets. Therefore, we assume that the mass change occurs uniformly over the ice sheet.	We use the estimates given in Meier et al. (2007); Meehl et al. (2007) and also allow for non-linear temporal variations in the mass changes in order to detect any acceleration in the ice mass changes.
G:	Mass changes in continental glaciers:	For the mass balance of the glaciers, most recent data sets should be used. Currently, the data set compiled by Dyurgerov (2002), which is available through the National Snow and Ice Data Center, appears to be best suited for estimating the LSL contribution in any location. The LSL fingerprint due to continental glaciers can be compute from eq. (10).	Estimates of future contributions of glaciers can be obtained if the mass balance of the glaciers can be predicted.

Table 1 continued.

V.	Process	Past sea levels	Future scenarios
L:	Mass transport in and mass exchange with the terrestrial hydrosphere	Currently, several models of the continental hydrosphere are available, most of them through the IERS Special Bureau for Hydrology. These hydrology models give the surface mass density of surface water, groundwater, and snow/ice on land, including the *Land Dynamics model* (LaD) of Milly & Shmakin (2002) and the *Global Land Data Assimilation Scheme* (GLDAS) of Rodell et al. (2004). Moreover, models derived from the NCEP and ECMWF reanalysis data also can serve for terrestrial water storage changes. In modeling the LSL effect of the hydrosphere by eq. (10), the total mass of the water cycle is an issue that needs attention.	Future changes in land water storage would have to come from climate models.
P:	Postglacial rebound:	The present-day signal of PGR in LSL can be predicted on the basis of geophysical models (e.g. Peltier, 1994). A suite of predictions is available at the IERS Special Bureau for Loading.	
V:	Vertical land motion:	Here we consider only vertical land motion that is not already included in the mass-related terms and PGR. Thus, we look mainly at tectonic processes including vertical deformation in seismic areas, subsidence due to sedimentation, and anthropogenic processes such as groundwater, oil, and gas extraction. This term could only be included on the basis of observations, but on a global scale, sufficient observations are not available.	

Table 2. Monthly mean sea-level records for tide gauges at the Dutch coast and adjacent coast. The records are those currently (2008/01/18) available in the PSMSL database (see http://www.pol.ac.uk/psmsl/). Stations marked with an asterisks are in the RLR data set. Only records longer than 20 years have been included. The column denoted by "Abbr." gives the station abbreviations used throughout this report. The column "Months" gives the number of monthly values actually available in the record. Trends are in mm/yr and for: b: total interval of the record, b_1: 1840-1950; b_2: 1950-2008; b_3: 1980-2008. Trends are determined in a fit of eq. 11 to the tide gauge record.

Station	Abbr.	Longitude	Latitude	Begin	End	Months	b	b_1	b_2	b_3
MAASSLUIS	MAA	4.250	51.917	1848	2005	1896	1.64	1.55	2.00	0.41
VLISSINGEN	VLI	3.600	51.450	1862	2005	1728	1.30	0.37	1.58	2.02
HOEK VAN HOLLAND	HOE	4.117	51.983	1864	2005	1704	2.38	2.60	2.83	1.52
DELFZIJL	DEL	6.933	53.333	1865	2005	1692	1.66	1.36	2.37	1.61
HARLINGEN	HAR	5.417	53.167	1865	2005	1692	1.36	1.60	1.43	0.44
DEN HELDER	DEN	4.750	52.967	1865	2005	1692	1.45	1.40	1.79	1.01
IJMUIDEN	IJM	4.583	52.467	1871	2005	1616	1.55	0.67	1.82	2.23
ZIERIKZEE	ZIE	3.917	51.633	1872	1986	1377	1.70	1.61	1.46	
HELLEVOETSLUIS	HEL	4.133	51.817	1861	1968	1296	1.58	1.51		
BROUWERSHAVEN	BRO	3.900	51.733	1872	1968	1164	1.64	1.35		
SHEERNESS	SHE	0.750	51.450	1832	2006	1062	1.74	0.88	1.84	2.08
WEST-TERSCHELLING	WES	5.217	53.367	1921	2005	1020	0.85	2.15	0.89	0.16
OOSTENDE	OOS	2.917	51.233	1937	2003	740		1.61	1.87	2.48
LOWESTOFT	LOW	1.750	52.467	1955	2006	594			2.33	3.55
SOUTHEND	SOU	0.733	51.517	1929	1983	587	1.21		0.06	
ZEEBRUGGE	ZEE	3.200	51.350	1942	2003	514			2.14	2.31
DOVER	DOV	1.317	51.117	1924	2006	513			2.30	1.51
BORKUM (FISCHERBALJE	BOR	6.667	53.583	1963	2002	480	4.94		4.94	5.19
NIEUWPOORT	NIE	2.717	51.150	1943	2003	466			3.01	2.85
EMDEN	EMD	7.217	53.383	1950	1986	444			0.36	
DUNKERQUE	DUN	2.367	51.050	1942	2004	425			1.85	
CALAIS	CAL	1.867	50.967	1941	2004	327				
STELLENDAM BUITEN	STE	4.033	51.833	1972	1995	287			3.29	
FELIXSTOWE	FEL	1.317	51.933	1917	2006	285				-0.92
NORDERNEY	NOR	7.150	53.717	1964	1986	276			1.11	
BROUWERSHAVENSE GAT	BRO	3.817	51.750	1980	2005	264				0.98
TILBURY	TIL	0.367	51.467	1929	1983	264			1.56	
HARWICH	HAR	1.283	51.950	1954	1976	251			1.70	
ROOMPOT BUITEN	ROO	3.667	51.617	1982	2005	240				1.12

Table 3. Secular trends and seasonality for tide gauges at the Dutch coast and adjacent coast. The time interval consider is 1958.0 to 2002.0. For each station, two rows are given, with the first one containing the results of a fit of eq. (11) to the data, and the second one the those of a fit of eq. (12). The last number in the first row is the difference in LSL trends that can be attributed to the atmospheric forcing. Atmospheric data is from ERA40 reanalysis. N: Number of monthly values. Standard LSQ errors of Sa and Ssa amplitudes are typically 0.1 mm, while phase errors are 0.1 degrees and 0.4 to 0.8 degrees for Sa and Ssa, respectively. For trends, these errors are typically between 0.1 and 0.2 mm/yr. For regression coefficients, typical errors are 0.1 mm/HPa for air pressure p and 0.1 mm/(m/s)^2 for the two horizontal wind stress components σ_{E} and σ_{N}.

Sta.	N	Sa		Ssa		Trend	Regression coefficients		
		mm	degree	mm	degree	mm/yr	p	σ_{E}	σ_{N}
DEL	492	86	158.5	20	123.85	2.05	0.85		
		63	165.0	13	178.7	1.20	-7.21	8.82	-2.74
WES	492	105	147.7	19	134.8	1.59	0.80		
		72	161.2	13	171.5	0.79	-7.30	5.84	-0.38
HAR	492	98	148.3	18	124.0	0.97	1.02		
		66	163.2	10	176.7	-0.05	-7.88	8.12	-1.62
DEN	492	99	149.4	18	138.0	1.70	0.82		
		73	164.5	12	172.4	0.88	-7.15	6.21	-1.18
IJM	492	92	155.4	16	136.5	1.59	0.86		
		74	172.5	12	172.8	0.73	-6.19	6.69	-1.83
HOE	492	75	152.3	17	139.1	3.23	0.55		
		61	165.7	12	156.2	2.68	-6.71	6.47	-3.21
MAA	492	66	147.9	17	126.6	2.25	0.60		
		53	161.8	10	143.7	1.65	-6.82	7.31	-3.78
VLI	492	71	157.3	14	156.3	1.24	0.31		
		60	170.6	11	175.5	0.93	-6.25	5.85	-2.70
OOS	492	66	156.9	15	162.1	1.59	0.05		
		58	166.9	11	168.2	1.54	-6.43	4.12	-2.17
LOW	468	66	160.3	13	159.4	1.70	-0.01		
		60	163.6	11	150.7	1.71	-3.28	1.91	-2.05
DOV	417	63	157.9	15	175.4	2.38	-0.05		
		59	164.2	11	164.5	2.43	-6.03	1.97	-1.06
ZEE	442	71	159.6	15	164.0	1.62	0.06		
		63	170.1	12	165.5	1.54	-5.55	4.53	-2.36
BOR	432	108	158.0	23	135.7	4.82	0.83		
		75	169.4	14	160.7	3.99	-6.79	7.31	-1.03
SHE	368	52	170.4	14	190.7	0.99	-0.33		
		59	161.4	10	168.3	1.32	-3.70	0.72	-2.96
NIE	394	68	147.6	15	160.9	2.60	-0.30		
		58	159.1	12	154.3	2.90	-6.99	4.22	-2.28
EMD	348	107	160.7	34	143.7	0.95	0.80		
		75	154.7	13	190.4	0.15	-7.89	10.66	-4.26
ZIE	345	72	157.2	24	159.3	1.79	0.67		
		59	166.5	13	183.2	1.12	-6.34	6.85	-3.70
DUN	325	79	154.2	18	170.4	1.19	-0.05		
		65	162.8	11	168.6	1.24	-6.36	3.55	-1.22
SOU	312	53	160.3	11	188.9	0.11	-0.01		
		59	157.7	8	181.9	0.12	-3.74	0.85	-3.16
TIL	264	38	142.2	11	178.0	1.56	-0.33		
		51	140.5	9	149.6	1.89	-4.29	-0.35	-3.39
STE	287	83	148.5	18	119.7	3.29	1.17		
		64	169.8	9	152.6	2.12	-6.71	7.41	-3.86
NOR	276	124	156.2	44	153.6	1.11	0.40		
		77	156.6	16	165.7	0.71	-7.42	7.82	-1.64
CAL	244	73	149.8	14	187.2	-3.66	-0.42		
		63	164.0	11	177.8	-3.24	-8.35	2.86	-0.34

Table 4. Vertical land motion rates for selected CGPS sites. The trends were determined in a LSQ fit of model eq. (11) to the GPS time series. Rates are with respect to ITRF2005 (Altamimi et al., 2007). N is the number of daily coordinate estimates in the time series, b the vertical trend in mm/yr. Positive trends indicate uplift. Least squares errors of the trends are typically between 0.01 and 0.05 mm/yr, but these errors are far too optimistic and therefore not given here.

Station	Longitude	Latitude	N	b
BORK	6.7474	53.5636	2322	-0.86
BORJ	6.6664	53.5789	795	-3.05
TERS	5.2194	53.3627	1221	-0.17
DELF	4.3876	51.9861	1184	0.43
DLFT	4.3876	51.9860	1739	0.64
DGLG	2.3448	50.9937	1393	1.68
SHEE	0.7434	51.4457	2438	1.48
HERT	0.3344	50.8675	1571	2.14

Table 5. Mass exchange of the ocean with other reservoirs in the global water cycle. All values are in mm/yr. Uncertainties of 12 are computed as the square root of the sum of squares of individual uncertainties.

N	Contribution	Period	Sea-level rise	Source
1	Glaciers and ice caps	1960-2000	0.41	Meier & Dyurgerov (2002)
2		1961-2003	0.50 ± 0.18	Bindoff et al. (2007)
3		2006	1.1 ± 0.24	Meier et al. (2007)
4	Greenland mass change	1950-1998	0.10 ± 0.05	Plag (2006c)
5		1961-2003	0.05 ± 0.12	Bindoff et al. (2007)
6		2006	0.5 ± 0.1	Meier et al. (2007)
7	Antarctic mass change	1950-1998	0.39 ± 0.11	Plag (2006c)
8		1961-2003	0.14 ± 0.41	Bindoff et al. (2007)
9		2006	0.17 ± 0.10	Meier et al. (2007)
10	Land water storage	1910-2000	-1.1 to 0.4	Church et al. (2001)
11			-0.35 ± 0.75	
12	2+5+8+11		0.34 ± 0.88	

Table 6. LSL balance for the Dutch tide gauges for the time window 1958-2002. The balance is as defined by eq. (5). Individual errors are ± 0.1 mm/yr for steric, ± 0.6 mm/yr for PGR, ± 0.65 mm/yr for Antarctica, and ± 0.13 mm/yr for Greenland. In total, the error of the balance is ± 0.90 mm/yr.

Station	LSL Trend	Atmosphere	Steric	PGR	Antarctica	Greenland	Balance
EMD	0.95	0.80	0.08	0.65	1.00	-0.28	-1.30
NOR	1.11	0.40	0.08	0.66	1.01	-0.28	-0.76
BOR	4.82	0.83	0.08	0.64	1.01	-0.28	2.54
WES	1.59	0.80	0.08	0.70	1.03	-0.28	-0.72
HAR	0.97	1.02	0.09	0.67	1.01	-0.28	-1.54
DEN	1.70	0.82	0.09	0.49	1.01	-0.28	-0.43
IJM	1.59	0.86	0.09	0.40	1.00	-0.26	-0.50
HOE	3.23	0.55	0.10	0.22	1.00	-0.24	1.61
MAA	2.25	0.60	0.10	0.21	1.00	-0.24	0.61
STE	3.29	1.17	0.09	0.15	1.00	-0.24	1.12
ZIE	1.79	0.67	0.09	0.10	1.00	-0.24	0.12
VLI	1.24	0.31	0.08	0.09	1.00	-0.24	0.00
ZEE	1.62	0.06	0.08	0.05	1.00	-0.24	0.67
OOS	1.59	0.05	0.07	0.01	1.00	-0.22	0.69
NIE	2.60	-0.30	0.07	-0.02	1.00	-0.22	2.07
DUN	1.19	-0.05	0.07	-0.05	1.00	-0.22	0.44
CAL	-3.66	-0.42	0.05	-0.07	0.99	-0.22	-3.99
DOV	2.38	-0.05	0.05	-0.05	1.00	-0.24	1.67
SHE	0.99	-0.33	0.06	-0.01	1.00	-0.26	0.53
SOU	0.11	-0.01	0.06	-0.01	1.00	-0.26	-0.67
TIL	1.56	-0.33	0.06	-0.01	1.00	-0.26	1.10
LOW	1.70	-0.01	0.07	0.05	1.03	-0.30	0.86

Table 7. PDF for the individual processes contributing to LSL variations at the Dutch coast.

Process	Variable	Mean	90% boundaries	
Atmospheric forcing	mean LSL	0 mm	± 50 mm	Oscillatory nature, times scales of 50-100 years
		50 mm	± 50 mm	Mean shift in wind and air pressure
Steric, currents	LSL trend	2 mm/yr	± 2 mm/yr	
PGR	LSL trend	0.5 mm/yr	± 0.6 mm/yr	Spatially variable
Greenland	LSL trend	0.5 mm/yr	± 0.1 mm/yr	Global, non-linear response possible
		-1.25 mm/yr	± 0.25 mm/yr	At Dutch coasts
Antarctica	LSL trend	0.17 mm/yr	± 0.08 mm/yr	Global, non-linear response possible
		0.44 mm/yr	± 0.21 mm/yr	At Dutch coasts
Glaciers and ice caps	LSL trend	1.1 mm/yr	± 0.24 mm/yr	Acceleration likely
Sea ice	LSL trend	?	?	Freshing effect, may be included in steric
Land water storage	LSL trend	0 mm/yr	± 0.4 mm/yr	Estimates are very uncertain
Vertical land motion	LSL trend	-1 to 3 mm/yr	± 1 mm/yr	Spatially variable

Table 8. Projections of future mean LSL trajectories resulting from realistic forcing scenarios. LSL increases are with respect to the level in 2000. Scenarios are S1: No accelerated melting, vertical land uplift of 1 mm/yr; S2: No accelerated melting, subsidence of 3 mm/yr; S3: As S1 but with increased melting of Greenland; S4: As S1 but with increased melting of Antarctica; S5: As S1 but with increased melting of glaciers and ice caps; S6: As S1 but with increased melting of Antarctica, glaciers and ice caps; S7: As S2 but with increased melting of Antarctica, glaciers and ice caps.

N	Factor	2050	2100	2200
1	Steric and ocean currents	100 ± 100	200 ± 200	400 ± 400
2	Atmosphere	0.0 ± 50	0 ± 50	0 ± 50
3	Greenland	-63 ± 13	-126 ± 26	-252 ± 52
4		-185 ± 80	-651 ± 282	
5	Antarctica	22 ± 11	44 ± 22	88 ± 22
6		53 ± 57	177 ± 177	
7	Glaciers and ice caps	55 ± 12	111 ± 27	222 ± 54
8		92 ± 45	255 ± 136	
9	Terrestrial hydrosphere	0 ± 20	0 ± 40	0 ± 80
10	PGR	25 ± 30	50 ± 60	100 ± 120
11	Vertical land motion	-50 ± 50	-100 ± 100	-200 ± 200
12		150 ± 50	300 ± 100	600 ± 200
S1	1+2+3+5+7+9+10+11	89 ± 129	179 ± 243	358 ± 479
S2	1+2+3+5+7+9+10+12	290 ± 129	579 ± 243	1158 ± 479
S3	1+2+4+5+7+9+10+11	-33 ± 151	-346 ± 373	
S4	1+2+3+6+7+9+10+11	120 ± 141	312 ± 301	
S5	1+2+3+5+8+9+10+11	126 ± 137	323 ± 277	
S6	1+2+3+6+8+9+10+11	157 ± 147	456 ± 329	
S7	1+2+3+6+8+9+10+12	358 ± 147	856 ± 329	

C Basic terms and concepts

We define LSL as the height h of the ocean surface above the underlying solid Earth, i.e.

$$h(\lambda,\theta,t) = \begin{cases} r_1(\lambda,\theta,t) - r_0(\lambda,\theta,t) & : \text{ in the ocean} \\ 0 & : \text{ on land} \end{cases}, \tag{6}$$

where r_0 and r_1 are the geocentric positions of the sea floor and sea level, respectively (Plag, 2006d). λ and θ are the geographical longitude and latitude, respectively. h is an absolute[6] quantity, independent of the reference frame used for r_0 and r_1. Therefore, the term *Relative Sea Level*, which is often used to refer to this quantity is a misnomer and not used here. Carefully maintained tide gauges, for which any relative movement of the tide gauge with respect to the underlying land is known, are the only tool to measure absolute LSL changes directly. Therefore, correcting tide gauge measurements of LSL for local vertical land motion does not lead to 'sea level' or 'absolute sea level changes' but to a different quantity, which is not easy to interpret or model.

We also define the geocentric position H of the sea surface as the distance of the sea surface from the *Center of Mass* (CM) of the Earth system (i.e. the solid Earth and its fluid envelop consisting of hydrosphere and atmosphere). This quantity is a relative quantity, which has to be given with respect to a geocentric reference frame, for example ITRF2000. Using another reference frame, for example ITRF2005, results in another sea surface position. Therefore, the sea surface position needs the frame information attached to it. Changes in the geocentric position of the (local) sea surface only coincide with LSL changes if the ocean floor at this position does not move vertically. The geocentric sea surface position as measured by satellite altimetry, is often referred to as 'geocentric sea level' or 'absolute sea level'. We consider these terms as misnomer and will not use them here.

For the discussion of the ocean's role in climate change and the global water cycle, we define two global absolute quantities, namely the volume V_{O} and the mass M_{O} of the ocean water. The volume is given by

$$V_{\mathrm{O}} = \int_{\mathrm{O}} \mathrm{d}V = \int_0^{2\pi}\int_0^{\pi}\left(\int_{r_0(\lambda,\vartheta)}^{r_1(\lambda,\vartheta)} r^2 dr\right)\sin\vartheta \mathrm{d}\vartheta\mathrm{d}\lambda, \tag{7}$$

where ϑ is the co-latitude. The ocean mass is given by

$$M_{\mathrm{O}} = \int_{\mathrm{O}} \rho \mathrm{d}V = \int_0^{2\pi}\int_0^{\pi}\left(\int_{r_0(\lambda,\vartheta)}^{r_1(\lambda,\vartheta)} \rho(\lambda,\vartheta,r) r^2 dr\right)\sin\vartheta \mathrm{d}\vartheta\mathrm{d}\lambda. \tag{8}$$

Both, V_0, M_0, and the density ρ are functions of time.

The mass M_{O} is an important quantity in the mass balance equation of the global water cycle, and the governing equation for mass changes can be written as

$$0 = \sum_{i=1}^{n} \frac{\mathrm{d}M_i}{\mathrm{d}t} = \sum_{i=1}^{n} \dot{M}_i, \tag{9}$$

where M_i is the total mass of the water in reservoir i and n the number of reservoirs in the global water cycle. Changes in M_{O} are solely determined by the scalar changes in the masses of the other reservoirs, independent of where the mass fluxes comes from or go to. Typical reservoirs in the global water cycle are the ocean, the atmosphere, the cryosphere and the water stored on land. The latter separates into a number of reservoirs including but not limited to surface water, soil moisture, groundwater, water stored in vegetation, and anthropogenic reservoirs.

There is no simple equation to relate changes in V_{O} or LSL to changes in the global water cycle. V_{O} is a complex function of M_{O}, the heat and salinity content of the ocean, and the distribution of the mass in the ocean. Changes in V_{O} result from the sum of steric changes, i.e. changes caused by temperature and salinity

[6] We refer here to quantities as *absolute quantities* if they do not depended on a specific reference frame chosen to refer them to.

changes of the sea water, and mass changes due to mass added to or subtracted from the ocean. Moreover, the density ρ of the sea water is a non-linear function of temperature, salinity and pressure (see e.g. Gill, 1982). Consequently, V_{O} depends not only on the amount but also the distribution of heat, mass and salinity in the ocean.

D LSL changes induced by mass redistribution

LSL changes caused by mass exchange of the ocean with other reservoirs in the global water cycle or by mass exchange between these reservoirs depend crucially on where the exchanged mass originates from. The equation, often referred to as the sea level equation, that links mass movements to LSL variations, was first introduced by Farrell & Clark (1976) in a simplified version:

$$\xi(\vartheta,\lambda,t) = c(t) + O(\vartheta,\lambda,t)\int_{-\infty}^{t}\int_{0}^{\pi}\int_{0}^{2\pi} G(\vartheta,\lambda,\vartheta',\lambda',t-t') \tag{10}$$

$$\frac{\mathrm{d}}{\mathrm{d}t'}\left\{O(\vartheta',\lambda',t')\rho_{\mathrm{W}}\xi(\vartheta',\lambda,t') + \left[1 - O(\vartheta',\lambda',t')\right]\rho_{\mathrm{L}}\eta(\vartheta',\lambda,t')\right\}\sin\vartheta'\mathrm{d}\lambda'\mathrm{d}\vartheta'\mathrm{d}t'.$$

where ξ is the LSL change (i.e. with respect to the deformable surface of the solid Earth), ϑ, λ, and t are co-latitude, longitude, and time, respectively, G is the Green's function for LSL, O the ocean function (which is 1 over the ocean and 0 over land), η the accumulated water or ice load change due to mass added to or removed from land, ρ_{W} and ρ_{L} are the densities of the ocean water and the load on land (water or ice), respectively, and $c(t)$ is a quantity included to ensure mass conservation. The Green's function accounts for the vertical motion of the land, the geoid changes caused by both the mass movements and the deformation of the solid Earth, and for the mass movements itself. Over the last decade, the sea level equation has been improved by several groups (e.g. Milne et al., 1999), and the most comprehensive and sophisticated version of the sea level equation is given by Mitrovica & Milne (2003). This equation accounts for meltwater inundation of deglaciated areas and includes rotational effects of LSL changes in a self-consistent manner.

Eq. (10) has been applied extensively to studies of LSL changes caused by the ice ages and the subsequent PGR (see e.g. Clark et al., 1978; Quinlan & Beaumont, 1982; Nakada & Lambeck, 1987; Tushingham & Peltier, 1992; Vermeersen & Sabadini, 1999). The disintegration of the last great ice sheets produced a distinct spatial pattern, a fingerprint, in LSL, with rather different temporal characteristics of the LSL in the near, intermediate and far field of the load changes (see, e.g., Quinlan & Beaumont, 1982; Lambeck, 1993). The elastic response of the Earth to present-day changes in the cryosphere can be expected to produce a similar fingerprint, which should be present in the tide gauge data. Nevertheless, using the same equation to describe the relation between present-day mass changes and LSL is restricted to a few examples (see e.g. Plag & Jüttner, 2001; Mitrovica et al., 2001; Plag, 2006c). In order to emphasize the importance of the fundamental relationship between any mass transport in the global water cycle and the LSL, we consider the case where the Greenland ice sheet increases while the Antarctic ice sheet melts with the two changes being exactly in balance. This mass movement will not induce any GSL change since the mass and volume of the ocean are constant, but LSL will change significantly over large regions with a LSL fall over most of the southern oceans, and a LSL increase over large parts of the northern hemisphere. Thus, the complex relation between LSL and ocean mass changes cannot be neglected in the interpretation of LSL observations in terms of GSL changes.

Eq. (10) assumes instantaneous distribution of the water in the global ocean and thus is only valid for sufficiently long time scales. Hydrodynamic studies showed that the equation is appropriate at annual to longer time scales (see Plag, 2006c, and the reference therein).

The Green's function G can be computed for a spherically symmetric, viscoelastic, isotropic Earth model (Peltier, 1974). Based on a Maxwell rheology and a simple Earth model, Farrell & Clark (1976) showed that the viscous contribution 1000 years after a significant mass change still is below a few percent of the instantaneous elasto-gravitative effect, with the fingerprint nearly unchanged by the viscous contribution. Nevertheless, a transient rheology may be important in the modeling of the response due to such a forcing on time scales of

centuries (Gasperini et al., 1986). However, up to multidecadal time scales, the viscous contribution can be consider small compared to the elasto-gravitative one.

The Green's function can be split into an elastic part describing the immediate response of the Earth to loading, and a viscous part accounting for time-delayed responses (e.g., Peltier, 1974). With respect to PGR, much focus has been on the viscous part, with the goal to determined the viscosity profile of the Earth mantle. Therefore, eq. (10) has been studied intensely for Maxwell rheologies (e.g., Peltier, 1974; Farrell & Clark, 1976; Clark et al., 1978; Nakada & Lambeck, 1987; Mitrovica et al., 1994a,b; Vermeersen et al., 1996), while the elastic response of the Earth to mass exchange between large ice masses and the ocean has only recently come into consideration (Plag & Jüttner, 2001; Mitrovica et al., 2001; Tamisiea et al., 2001; Plag, 2006c). Unlike in the case of the sea level equation, the elastic response of the solid Earth to tidal forcing has been studied in detail (e.g., Love, 1909, 1911; Dahlen, 1972; Wilhelm, 1986). Likewise, ocean tidal loading (e.g., Farrell, 1972; Scherneck, 1991) and non-tidal loading due to atmospheric, ocean and terrestrial hydrosphere have been studied in great detail (e.g., Farrell, 1972; Rabbel & Zschau, 1985; van Dam et al., 2001). In all these cases, an approach based on *Load Love Numbers* (LLN)(see, e.g., Farrell, 1972; Wilhelm, 1986, for details) has been applied. These LLNs are either used to compute Green's functions for the desired quantity (surface displacements, gravity changes, tilt, strain, etc.) or to compute the effects by a weighted sum of the spherical harmonic expansion of the load.

For elastic body tide Love Numbers and LLNs, results of most groups show reasonable agreement (see Figure 8 for LLNs). However, the fingerprints computed by Plag & Jüttner (2001) and Mitrovica et al. (2001) for the large ice sheets show large differences. Therefore, in the following we will given an overview of the potential sources of these differences. These differences can be in the Earth model, the computation of the LLNs, the computation of the desired quantities, and, in the case of the sea level equation, the solution of the integral equation. Unfortunately, up to now, no rigorous comparison of the solution of the sea level equation for the elastic case has been done between groups.

Earth model: For solid Earth tides and loading studies, the Earth model most often used is the *Preliminary Earth Reference Model* (PREM), which is a visco-elastic spherically symmetric Earth model derived mainly from seismic wave data and free oscillations (Dziewonski & Anderson, 1981). The parameters of the PREM (density, bulk and shear modulus) are given as polynomials in the radius for x layers. The main period of the observations is close to 30 s (Zschau, 1986), and the elastic moduli need to be derived. Small differences can result from the choice of rheology used to determine the elastic moduli (Plag & Jüttner, 1996). The PREM has a global ocean of 3000 m depth, which for computation of LLNs needs to be replaced by a solid layer. The choice of the elastic parameters for this layer can also impact the LLNs, particularly for higher degree and order. An important question is whether the Earth model is compressible or not. Plag & Jüttner (2001) use a compressible Earth model, but it is not clear whether this is also the case for Mitrovica et al. (2001).

Computation of LLN: For the computation of the LLN, an integration of the equation of linear momentum is required from the Earth's center to the surface (Wang, 1991, e.g.,). For this integration, the elastic parameters of the Earth model need to be parametrized as function of radius. In most cases, this is done with a number of homogeneous layers with constant parameters (density, bulk and shear moduli). In case of a compressible medium this leads to an inconsistency since density of a homogeneous, selfgravitating medium would increase with depth due to increasing pressure. Therefore, Wang (1991) made the choice to represent the parameters as polynomials in radius. This approach was also used by Plag & Jüttner (2001). To our knowledge, this is the only group who applies this solution, while all other groups use homogeneous and most likely incompressible layers.

Convolution: For computation of loading signals, two apporaches have been used, namely a spatial convolution of the Green's function with the surface load, and a summation of the spherical harmonic expansion of the load weighted with the LLNs. As pointed out by Van Dam et al. (2003), the differences in the computed effects due to these two numerical approaches are very small.

Solution of the sea level equation: The standard apporach to the solution of the sea level equation is an iteration, which starts with a uniform distribution of the melt water over the ocean. Further iterations lead then to a non-uniform distribution of the water masses (see, e.g., Clark et al., 1978; Quinlan & Beaumont, 1982;

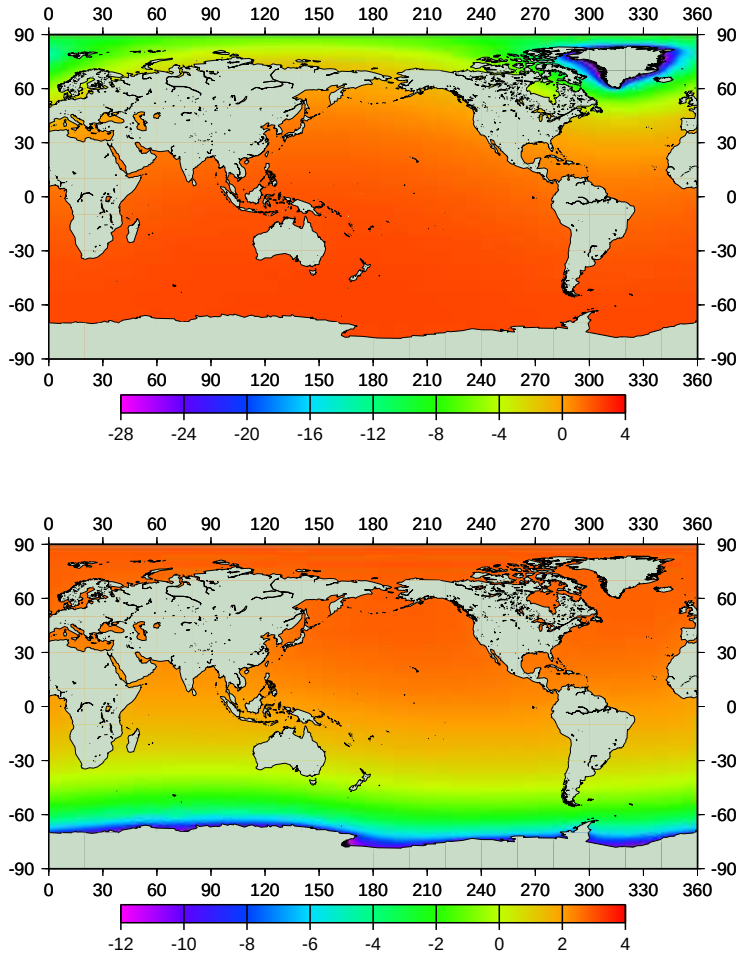

Figure 12. LSL fingerprints of mass changes in the large ice sheets. The fingerprints are relative to the GSL change induced by a uniform mass change across the ice sheet. Upper diagram: Greenland: Melting of one meter of ice results in a GSL rise of ∼5 mm. However, close to the ice sheet LSL will fall by more than 100 mm while farfield increase in LSL can reach as much as 13 mm. Lower diagram: Antartica: Melting of one meter of ice results in a GSL rise of ∼38 mm. However, close to the ice sheet LSL will fall by more than 400 mm while farfield increase in LSL can reach as much as 100 mm.

Nakada & Lambeck, 1987, for a discussion of the iteration). However, to our knowledge, it has not been shown rigorously that the iteration actually converges to the solution of the integral equation. Plag & Jüttner (2001) used a different approach and inverted the integral equation directly for the coefficients of the load distribution. However, due to the large number of coefficients in the spherical harmonic expansion of the water load, they were limited to degree and oder of ∼70.

The global fingerprints of the two largest ice sheets computed by Plag & Jüttner (2001) are shown in Fig. 12. The fingerprints emphasize the large spatial variability and the large deviation LSL can exhibit from the GSL change. It is noted here that the exact details of the fingerprint depend on the Earth model used for the computations. The fingerprints computed, for example, by Mitrovica et al. (2001) show significant deviations from those given here. The fingerprints of Plag & Jüttner (2001) show larger spatial variability and the angular distance between the ice load and areas with a positive response is much much larger than for the fingerprints computed by Mitrovica et al. (2001). As discussed above, the causes of these differences can be in the parameterization of the Earth model, differences in the LLNs, and differences in the solution of the sea level equation.

E Regression analysis

For each tide gauge, Plag (2006c) determined a secular trend by fitting the model function

$$g(t) = a + bt + \sum_{i=1}^{2} A_i \sin(\omega_i t + \phi_i) \tag{11}$$

to the series of monthly mean sea levels, where t is time, a is an offset and b the constant secular LSL trend. A_i and ϕ_i are the amplitude and phase, respectively, of an annual and semiannual constituent. In the fit, the parameters a and b and the amplitudes of the sine and cosine terms of the annual and semi-annual constituents are determined simultaneously.

Here we use an alternative equation to determine the LSL trends, i.e.

$$g(t) = a + bt + \sum_{i=1}^{2} A_i \sin(\omega_i t + \phi_i) + \sum_{i=1}^{3} d_i \sigma_i \tag{12}$$

where $\sigma_i,\ i = 1, 2, 3$, are the relevant components of the atmospheric stress tensor on the sea surface, and d_i are the respective regression coefficients, which we determine together with the other parameters in the least squares fit to the LSL records. The component of the atmospheric stress tensor perpendicular to the sea surface is the air pressure p. The horizontal components are taken to be proportional to the wind stress components, i.e.

$$\sigma_2 \sim w_{\mathrm{E}} \sqrt{w_{\mathrm{E}}^2 + w_{\mathrm{N}}^2} \tag{13}$$

$$\sigma_3 \sim w_{\mathrm{N}} \sqrt{w_{\mathrm{E}}^2 + w_{\mathrm{N}}^2} \tag{14}$$

where w_{E} and w_{N} are the east and north components of the wind vector, respectively. We denote the sets of LSL trends determined with eq. (11) and eq. (12) as T1 and T2, respectively.

Monthly mean values of the air pressure and the wind stress components are computed from the ERA40 reanalysis data provided by the *European Center for Medium Range Weather Forecast* (ECMWF). The ERA40 data set has a spatial and temporal resolution of $2.5^\circ \times 2.5^\circ$ and 6 hours, respectively. Monthly means of σ_2 and σ_3 are computed as averages of the six-hourly values of these quantities.

References

Altamimi, Z., Collilieux, X., Legrand, J., Garayt, B., & Boucher, C., 2007. ITRF2005: A new release of the International Terrestrial Reference Frame based on time series of station positions and Earth Orientation Parameters, *J. Geophys. Res.*, **112**, B09401, doi:10.1029/2007JB004949.

Aoyama, Y., Naito, I., Iwabuchi, T., & Yamazaki, N., 2003. Atmospheric quasi-14 month fluctuations and excitation of the Chandler wobble, *Earth Planets Space*, **55**, e25–e28.

Bindoff, N. L., Willebrand, J., Artale, V., Cazenave, A., Gregory, J., Gulev, S., Hanawa, K., Le Qur, C., Levitus, S., Nojiri, Y., Shum, C., Talley, L., & Unnikrishnan, A., 2007. Observations: Oceanic climate change and sea level, in *Climate Change 2007: The Physical Science Basis. Contribution of Working Group I to the Fourth Assessment Report of the Intergovernmental Panel on Climate Change*, edited by S. Solomon, D. Qin, M. Manning, Z. Chen, M. Marquis, K. B. Averyt, M. Tignor, & H. L. Miller, Cambridge University Press, Cambridge, United Kingdom and New York, NY, USA.

Cartwright, D. E. & Edden, A. C., 1973. Corrected tables of tidal harmonics, *Geophys. J. R. Astron. Soc.*, **33**, 253–264.

Chelton, D. B. & Enfield, D. B., 1986. Ocean signals in tide gauge records, *J. Geophys. Res.*, **91**, 9081–9098.

Church, J. A., Gregory, J. M., Huybrechts, P., Kuhn, M., Lambeck, K., Nhuan, M. T., Qin, D., & Woodworth, P. L., 2001. Changes in sea level, in *Climate Change 2001: The Scientific Basis. Contribution of Working Group I to the Third Assessment Report of the Intergovernmental Panel on Climate Change*, edited by J. T. Houghton, Y. Ding, D. J. Griggs, M. Noguer, P. J. van der Linden, X. Dai, K. Maskell, & C. A. Johnson, pp. 639–693, Cambridge University Press, Cambridge.

Clark, J. A., Farrell, W., & Peltier, W. R., 1978. Global changes in postglacial sea level: A numerical calculation., *Quatern. Res.*, **9**, 265–287.

Dahlen, F. A., 1972. Elastic dislocation theory for a self-gravitating elastic configuration with an initial static stress field, *Geophys. J. R. Astron. Soc.*, **28**, 357–383.

Dyurgerov, M., 2002, updated 2005. Glacier mass balance and regime measurements and analysis, 1945-2003, Tech. rep., Edited by M. Meier and R. Armstrong. Institute of Arctic and Alpine Research, University of Colorado, Boulder, Co., Distributed by National Snow and Ice Data Center, Boulder, CO.

Dziewonski, A. M. & Anderson, D. L., 1981. Preliminary reference Earth model, *Phys. Earth Planet. Int.*, **25**, 297–356.

Farrell, W. E., 1972. Deformation of the Earth by surface loads., *Rev. Geophys. Space Phys.*, **10**, 761–797.

Farrell, W. E. & Clark, J. A., 1976. On postglacial sea level, *Geophys. J. R. Astron. Soc.*, **46**, 647–667.

Gasperini, P., Sabadini, R., & Yuen, D. A., 1986. Excitation of the earth's rotational axis by recent glacial discharges, *Geophys. Res. Lett.*, **13(6)**, 533–536.

Gill, A. E., 1982. *Atmosphere-Ocean Dynamics*, Academic Press.

Hulme, M., Xianfu Li, Tumpenny, J., Mitchell, T., Jenkins, G., Jones, R., Lowe, J., Murphy, J., Hassel, D., Boorman, P., McDonald, R., & Hills, S., 2002. Climate change scenarios for the united kingdom: The ukcipo2 scientific report, Tech. rep., Tyndall Centre fro Climate Change Research, School of Environmental Sciences, University of East Anglia, Norwich, UK, 120 pp.

Hurrell, J. W., 1995. Decadal trends in the North Atlantic Oscillation: regional temperatures and precipitation, *Science*, **269**, 676–679.

Hurrell, J. W. & van Loon, H., 1997. Decadal variations in climate associated with the North Atlantic Oscillation, *Climatic Change*, **36**, 301–326.

Ishii, M., Kimoto, M., & Kachi, M., 2003. Historical ocean subsurface temperature analysis with error estimates, *Monthly Weather Rev.*, **131**, 51–73.

Lambeck, K., 1993. Glacial rebound of the British Isles - I. Preliminary model results, II. A high-resolution, high precision model, *Geophys. J. Int.*, **115**, 941–990.

Levitus, S., Antonov, J., Boyer, T., & Stephens, C., 2000. Warming of the world ocean, *Science*, **287**, 2225–2229.

Levitus, S., Stephens, C., Antonov, J., & Boyer, T., 2000. Yearly and year-season upper ocean temperature anomaly field, 1948-1998, Tech. rep., U.S. Gov. Printing Office, Washington, D.C.

Levitus, S., Antonov, J., & Boyer, T., 2005. Warming of the world ocean, 1955-2003, *Geophys. Res. Lett.*, **32**, doi:10.1029/2004GL021592.

Love, A. E. H., 1909. The yielding of the earth to disturbing forces, *Proc. Royal Soc. London, Ser. A.*, **82**, 73–88.

Love, A. E. H., 1911. *Some problems of geodynamics*, Cambridge University Press, Cambridge.

Marbaix, P. & Nicholls, R. J., 2007. Accurately determining risk of rising sea levels, *Eos, Trans. Am. Geophys. Union*, **88**(43), 441–442.

Meehl, G. A., Stocker, T. F., Collins, W. D., Friedlingstein, P., Gaye, A. T., Gregory, J. M., Kitoh, A., Knutti, R., Murphy, J. M., Noda, A., Raper, S. C. B., Watterson, I. G., Weaver, A., & Zhao, Z.-C., 2007. Global climate projections, in *Climate Change 2007: The Physical Science Basis. Contribution of Working Group I to the Fourth Assessment Report of the Intergovernmental Panel on Climate Change*, edited by S. Solomon, D. Qin, M. Manning, Z. Chen, M. Marquis, K. B. Averyt, M. Tignor, & H. L. Miller, Cambridge University Press, Cambridge, United Kingdom and New York, NY, USA.

Meier, M. F. & Dyurgerov, M. B., 2002. How Alaska affects the world, *Science*, **297**, 350–351.

Meier, M. F., Dyurgerov, M. B., Rick, U. K., O'Neel, S., Pfeffer, W. T., Anderson, R. S., & Glazovsky, A. F., 2007. Glaciers dominated eustatic sea-level rise in the 21st century, *Science*, **317**, 1064–1067.

Milly, P. C. D. & Shmakin, A. B., 2002. Global modeling of land water and energy balances. Part I: The land dynamics (LaD) model, *J. Hydrometeorology*, **3**, 283–299.

Milne, G. A., Mitrovica, J. X., & Davis, J. L., 1999. Near-field hydro-isostasy: the implementation of a revised sea-level equation, *Geophys. J. Int.*, **139**, 464–482.

Mitrovica, J. X. & Milne, G. A., 2003. On post-glacial sea level: I. General theory, *Geophys. J. Int.*, **154**, 253–267.

Mitrovica, J. X., Davis, J. L., & Shapiro, I. I., 1994. A spectral formalism for computing three-dimensional deformations due to surface loads 1.Theory, *J. Geophys. Res.*, **99**, 7057–7073.

Mitrovica, J. X., Davis, J. L., & Shapiro, I. I., 1994. A spectral formalism for computing three-dimensional deformations due to surface loads 2.Present-day glacial isostatic adjustment, *J. Geophys. Res.*, **99**, 7075–7101.

Mitrovica, J. X., Tamisiea, M. E., Davis, J. L., & Milne, G. A., 2001. Recent mass balance of polar ice sheets inferred from patterns of global sea-level change, *Nature*, **409**, 1026–1028.

Nakada, M. & Lambeck, K., 1987. Glacial rebound and relative sea-level variations: a new appraisal., *Geophys. J. R. Astron. Soc.*, **90**, 171–224.

Peltier, W. R., 1974. The impulse response of a Maxwell Earth, *Rev. Geophys. Space Phys.*, **12**, 649–669.

Peltier, W. R., 1994. Ice age paleotopography, *Science*, **265**, 195–201.

Peltier, W. R., 2004. Global glacial isostasy and the surface of the ice-age Earth: The ICE-5G(VM2) model and GRACE, *Ann. Rev. Earth Planet Sci.*, **32**, 111–149.

Philander, S. G. H., 1990. *El Niño, La Niña and the Southern Oscillation*, Academic Press, San Diego, CA.

Plag, H.-P., 1997. Chandler wobble and pole tide in relation to interannual atmosphere-ocean dynamics, in *Tidal Phenomena*, edited by H. Wilhelm, W. Zürn, & H.-G. Wenzel, no. 66 in Lecture Notes in Earth Sciences, pp. 183–218, Springer.

Plag, H.-P., 2000. Large-scale phenomena on interannual to interdecadal time scales detected from tide gauges and atmospheric data, in *Ocean Circulation Science derived from the Atlantic, Indian and Arctic Sea Level Networks*, edited by G. Mitchum, Workshop Report No. 171, pp. 4–8, Intergovernmental Oceanographic Commission.

Plag, H.-P., 2006. GEO, GEOSS and IGOS-P: The framework of global Earth observations, in *The International GNSS Service (IGS): Perspectives and Visions for 2010 and beyond*, edited by T. Springer, G. Gendt, & J. M. Dow, pp. 11, invited abstract.

Plag, H.-P., 2006. National geodetic infrastructure: current status and future requirements - the example of Norway, Bulletin 112, Nevada Bureau of Mines and Geology, University of Nevada, Reno, 97 pages.

Plag, H.-P., 2006. Recent relative sea level trends: an attempt to quantify the forcing factors, *Phil. Trans. Roy. Soc. London, A*, **364**, 1841–1869.

Plag, H.-P., 2006. Concepts in global and local sea level studies, *Global Planetary Change*, In preparation.

Plag, H.-P., 2006. Estimating recent global sea level changes, in *Dynamic Planet – Monitoring and Understanding a Dynamic Planet with Geodetic and Oceanographic Tools*, edited by P. Tregoning & C. Rizos, vol. 130 of **International Association of Geodesy Symposia**, pp. 39–46, Springer Verlag, Berlin.

Plag, H.-P. & Jüttner, H.-U., 1996. Determination of three-dimensional Earth models using geodetic observations: Problems and perspective, *Eos, Trans. Am. Geophys. Union*, **77**(46), F131, Invited abstract, AGU Fall Meeting.

Plag, H.-P. & Jüttner, H.-U., 2001. Inversion of global tide gauge data for present-day ice load changes, in *Proceed. Second Int. Symp. on Environmental research in the Arctic and Fifth Ny-Ålesund Scientific Seminar*, edited by T. Yamanouchi, no. Special Issue, No. 54 in Memoirs of the National Institute of Polar Research, pp. 301–317.

Plag, H.-P., Blewitt, G., & Herring, T. A., 2007. Towards a consistent conventional treatment of surface-load induced deformations, Position Paper presented at the IERS Workshop on Conventions, September 20-21, 2007, Sevres, France. Available at http://www.bipm.org/en/events/iers/papers.html.

Quinlan, G. & Beaumont, C., 1982. The deglaciation of Atlantic Canada as reconstructed from the post glacial relative sea-level record, *Can. J. Earth Sci.*, **19**, 2232–2246.

Rabbel, W. & Zschau, J., 1985. Static deformations and gravity changes at the Earth's surface due to atmospheric loading, *J. Geophys. Res.*, **56**, 81–99.

Rodell, M., Houser, P. R., Jambor, U., Gottschalck, J., Mitchell, K., Meng, C.-J., Arsenault, K., Cosgrove, B., Radakovich, J., Bosilovich, M., Entin, J. K., Walker, J. P., Lohmann, D., & Toll, D., 2004. The Global Land Data Assimilation System, *Bull. Amer. Meteor. Soc.*, **85**(3), 381–394.

Scherneck, H.-G., 1991. A parameterised solid earth tide model and ocean tide loading effects for global geodetic measurements, *Geophys. J. Int.*, **106**, 677–694.

Schlesinger, M. E. & Ramankutty, N., 1994. An oscillation in the global climate system of 65-70 years, *Nature*, **367**, 723–726.

Spencer, N. E. & Woodworth, P. L., 1993. Data holdings of the Permanent Service for Mean Sea Level, Tech. rep., Permanent Service for Mean Sea Level, Bidston, UK, 81pp.

Stroeve, J., Serreze, M., Gearheard, S., Holland, M., Maslanik, J., Meier, W., & Scambos, T., 2008. Arctic Sea ice extent plummets in 2007, *Eos, Trans. Am. Geophys. Union*, **89**(2), 13–14.

Tamisiea, M. E., Mitrovica, J. X., Milne, G. A., & Davis, J. L., 2001. Global geoid and sea level changes due to present-day ice mass fluctuations, *J. Geophys. Res.*, **106**(B12), 30,849–30,864.

Tamura, Y., 1987. A harmonic development of the tide-generating potential, *Bull. Inf. Marées Terrestres*, **99**, 6813–6855.

Tedesco, M., 2007. A new record in 2007 for melting in Greenland, *Eos, Trans. Am. Geophys. Union*, **88**(39), 383.

Thomas, R., Rignot, E., Casassa, G., Kanagaratnam, P., Acuna, C., Akins, T., Brecher, H., Frederick, E., Gogineni, P., Kabill, W., Manizade, S., Ramamoorthy, H., Rivera, A., Russell, R., Sonntag, J., Swift, R., Yungle, J., & Zwally, J., 2004. Accelerated sea-level rise from West Antarctica, *Science*, **306**, 255–258.

Thompson, D. W. J. & Wallace, J. M., 2001. Regional climate impacts of the Northern Hemisphere annular mode and associated climate trends, *Science*, **293**, 85–89.

Trupin, A. & Wahr, J. M., 1990. Spectroscopic analysis of global tide gauge sea level data, *Geophys. J. Int.*, **100**, 441–453.

Tsimplis, M. N., Álvarez-Fanjul, E., Gomis, D., Fenoglio-Marc, L., & Pérez, B., 2005. Mediterranean sea level trends: Atmospheric pressure and wind contribution, *Geophys. Res. Lett.*, **32**, doi:10.1029/2005GL023867.

Turner II, B. L., Clark, W. C., Kates, R. W., Richards, J. F., Mathews, J. T., & Meyer, W. B., eds., 1990. *The Earth as Transformed by Human Action: Global and Regional Changes in the Biosphere Over the Past 300 Years*, University Press, Cambridge, 713 pages.

Tushingham, A. M. & Peltier, W. R., 1992. Validation of the ICE-3G model of Würm-Wisconsin deglaciation using a global data base of relative sea level histories, *J. Geophys. Res.*, **97**, 3285–3304.

Van Dam, T., Plag, H.-P., Francis, O., & Gegout, P., 2003. GGFC Special Bureau for Loading: current status and plans, in *Proceedings of the IERS Global Geophysical Fluid Center Workshop, Munich, November 20-21, 2002*, edited by B. Richter, W. Schwegman, & R. Dick, no. 30 in International Earth Rotation and Reference System Service, IERS Technical Note, pp. 180–198.

van Dam, T. M., Wahr, J., Milly, P. C. D., Shmakin, A. B., Blewitt, G., Lavalee, D., & Larson, K. M., 2001. Crustal displacements due to continental water loading, *Geophys. Res. Lett.*, **28**, 651–654.

Vaughan, D. G., Holt, J. W., & Blankenship, D. D., 2007. West Antarctic links to sea level estimation, *Eos, Trans. Am. Geophys. Union*, **88**(46), 485–486.

Vermeersen, L. L. A. & Sabadini, R., 1999. Polar wander, sea-level variations and Ice Age cycles, *Surv. Geophys.*, **20**, 415–440.

Vermeersen, L. L. A., Sabadini, R., & Spada, G., 1996. Analytical visco-elastical relaxation models, *Geophys. Res. Lett.*, **23**, 697–700.

Wadhams, P. & Munk, W., 2004. Ocean freshening, sea level rising, sea ice melting, *Geophys. Res. Lett.*, **31**, doi:10.1029/2004GL020039.

Wang, R., 1991. *Tidal deformations on a rotating, spherically asymmetric, visco-elastic and laterally heterogeneous Earth*, vol. 5 of **European University Studies, Series XVII,Earth Sciences**, Peter Lang, Frankfurt am Main, 112pp.

Wilhelm, H., 1986. Spheroidal and torsional global response functions, *J. Geophys.*, **59**, 16–22.

Woodworth, P. & Player, R., 2003. The Permanent Service for Mean Sea Level: an update to the 21st century, *J. Coastal Research*, **19**, 287–295.

Zschau, J., 1986. Tidal friction in the solid Earth: Constraints from the Chandler wobble period, in *Space Geodesy and Geodynamics*, edited by A. J. Anderson & A. Cazenave, pp. 315–346, Academic Press Inc. (London) Ltd.

Zwally, H. J., Abdalati, W., Herring, T., Larson, K., Saba, J., & Steffen, K., 2002. Surface melt-induced acceleration of greenland ice-sheet flow, *Science*, **297**, 218–222.